Engineering of Substrate Surface for the Synthesis of Ultra-Thin Composite Pd and Pd-Cu Membranes for H_2 Separation

by

Federico Guazzone

A PhD thesis

Submitted to the faculty of the

Worcester Polytechnic Institute

In fulfillment of the requirements for the

Degree of Doctor of Philosophy

In Chemical Engineering

by

December 2005

APPROVED:

Dr. Yi Hua Ma, Advisor	Dr. David DiBiasio, Interim Head of Department
Dr. Nikolaos K. Kazantzis, Committee Member	
Dr. Satya Shivkumar, Committee Member	

To my family

Acknowledgements

I would like to express my sincere gratitude to my advisor Prof. Yi Hua Ma for the time he spent explaining to me physical concepts and the time he awarded me to understand them. The assimilation of a concept needs reasoning and a lot of maturation and I am thankful to Prof. Ma in understanding and respecting these maturation times in all of his students. The models, concepts and ideas exposed in this thesis are the fruit of many Saturday after-noon conversations that Prof. Ma and I had during the four years of my PhD work at Worcester Polytechnic Institute. I hope he enjoyed, as much as I did, all those fruitful scientific conversations. I particularly appreciated the freedom Prof. Ma accorded to all of us in our research. I am very grateful to the committee members Prof. Nikolaos Kazantzis and Prof. Satya Shivkumar for their suggestions and valuable comments.

I also would like to thank Dr. Erik Engwall and Dr. Ivan Mardilovich for giving me the valuable technical and experimental knowledge a student needs at the beginning of his PhD to build new set-ups and conceive new experiments for his research. I would like to thank Jack Ferraro and Doug White for the great help they provided in building the experimental set-ups used during my research years. I also would like to thank Engin, Raj, Alpna, Natalie, Mike, Diana and Ceylan for the scientific and philosophical conversations that made this experience worthwhile and most of all, enjoyable.

I particularly would like to thank Dr. Andrew Payzant and Dr. Scott Speakman at the High Temperature Materials Laboratory in Oak Ridge National Laboratories for making my visits to html so fruitful. Larry Walker and Tom Geer are also acknowledged for their expertise in microscopic techniques and sample preparation for electron microscopy. The important physical concepts learnt at the html were determinant for my research.

Sincere appreciation is expressed to the Shell team, especially Dr. Andreas Matzakos, for all meetings rich in science, technique and ideas. The financial and technical support for this project from Shell International Exploration and Production, Inc. and Shell Hydrogen is sincerely acknowledged.

Appreciation is expressed to the entire Chemical Engineering Department and staff for making my research a rewarding experience and Diana Johnson for her great talents in finding the old, but very interesting, publications that I needed.

I believe that leaving my country and coming to this new land to pursue a doctoral degree would have been hardly possible without Majo's and Erik's friendship. I express my sincere gratitude to Majo, Diana, Luis and Prof. Ma to support me and help me during the interesting time it took to write the thesis.

I dedicate this work to my family, which was always there, in the very good times as well as in the difficult times.

Abstract

This work describes a new technique to prepare ultra-thin composite Pd–Porous Metal (PM) membranes for H_2 separation. This technique consists of the gradual smoothing of the PM support's surface with several layers of pre-activated alumina particles of different sizes. The deposition of coarse, fine and ultra-fine alumina particles resulted in the narrowing of the PM support's surface pore size distribution. The surface smoothness achieved after the grading of the PM support's surface allowed for the preparation of gas tight Pd layers as thin as 5.6μm. The Pd layers were very uniform due to the presence of the grade layer and strongly attached to the support.

Composite Pd membranes prepared on graded supports showed H_2 permeance as high as 50 $m^3/(m^2\ h\ bar^{0.5})$ at 500ºC and ideal selectivities (H_2/He) as high as 27000. Moreover, the H_2 permeance and ideal selectivity were stable over 1100 hr at 500ºC in H_2 atmosphere. Composite Pd-Cu membranes showed H_2 permeance as high as 30 $m^3/(m^2\ h\ bar^{0.5})$ at 450ºC and ideal selectivities (H_2/He) as high as 900. The H_2 permeance and ideal selectivity of Pd-Cu membranes were stable over 500 hr at 450ºC in H_2 atmosphere. The long-term H_2 permeance and ideal selectivity stability of all composite Pd and Pd-Cu membranes represents a breakthrough in composite Pd membrane synthesis.

Executive summary

The analysis carried along this dissertation provides a thorough understanding of a new technology available for the preparation of composite Pd and Pd alloy membranes on Porous Metal (PM) supports. This new technique consists of the gradual smoothing of the PM support's surface with several layers of pre-activated alumina particles of different sizes. The deposition of coarse, fine and ultra-fine alumina particles resulted in the narrowing of the PM support's surface pore size distribution. The surface smoothness achieved after the grading of the PM support's surface allowed for the preparation of gas tight Pd layers as thin as 5.6μm. The Pd layers were very uniform due to the presence of the grade layer and strongly attached to the support. SEM investigations of the Pd-engineered supports interface revealed that the grade layer was only located at the pores mouth. Composite Pd membranes prepared on graded supports showed H_2 permeance as high as 50 $m^3/(m^2\ h\ bar^{0.5})$ at 500ºC and ideal selectivities (H_2/He) as high as 27000. Moreover, the H_2 permeance and ideal selectivity were stable over 1100 hr at 500ºC in H_2 atmosphere. Composite Pd-Cu membranes showed H_2 permeance as high as 30 $m^3/(m^2\ h\ bar^{0.5})$ at 450ºC and ideal selectivities (H_2/He) as high as 900. The H_2 permeance and ideal selectivity of Pd-Cu membranes were stable over 500 hr at 450ºC in H_2 atmosphere. The long-term H_2 permeance and ideal selectivity stability of all composite Pd and Pd-Cu membranes represents a breakthrough in composite Pd membrane synthesis.

The alloying of Pd-Cu bi-layers and the ordering transformation taking place in PdCu alloys were studied by means of High temperature X-Ray Diffraction (HTXRD) analysis. Experimental results showed that alloying of Pd-Cu bi-layers occurred by the diffusion of Cu into Pd. Also, it was found that the ordering fcc to bcc transformation taking place in PdCu alloys did not rely on the diffusion of metallic elements to occur i.e. the ordering transformation was a diffusionless transformation.

This study also focused on the elucidation of the intermetallic diffusion phenomenon encountered in composite Pd-Porous Stainless Steel (PSS) membranes. By measuring the kinetics at which the H_2 flux declined at every temperature, two mechanisms were identified: (1) the first one occurring at low temperatures (<500ºC) and attributed to the diffusion of Fe through the grain boundaries of Pd and, (2) the second one occurring at high temperatures (>500ºC) attributed to the diffusion of Fe through the lattice of Pd.

The thermal stresses arising from the mismatch in the coefficient of thermal expansion between the Pd film and the support were determined by means of x-ray diffraction. The results indicated that the release of stresses began to occur at temperatures close to 400ºC. Also, the release of stresses took place with a visible sintering of Pd clusters within the thin Pd film. The stresses due to the absorption of H_2 were also studied and modeled. It was estimated that the maximum compressive stress under which these composite Pd membranes were during H_2 characterization was equal to 260 MPa.

Finally, the mechanism leading to selectivity decline was studied. Although composite Pd membranes showed high selectivities (H_2/He) values (>10000 at temp. <400ºC), their selectivity slowly declined at 450 and 500ºC. The energy the system needed to lead to the

growth of leaks was equal to 237 $kJmol^{-1}$, which closely matched the activation energy of sintering.

Table of contents

Acknowledgements ... *iii*
Abstract ... *v*
Executive summary ... *vi*
Table of contents ... *ix*
List of figures ... *xiii*
List of tables ... *xx*

1 Introduction 1

2 Literature review 9

2.1 Pd and Pd-alloys systems ... 9
2.2 Methods of Pd deposition onto porous substrates ... 17
2.3 Electroless deposition of Pd and Pd alloys coatings ... 20
2.3.1 Activation of the substrate 20
2.3.2 The chemistry of Pd deposition 22
2.4 Composite Pd and Pd alloy membranes ... 24
2.4.1 Supports and diffusion barriers used for metal composite membranes 24
2.4.2 Asymmetric supports 27
2.4.3 The use of an external driving force during deposition 29
2.5 The microstructure of Pd thin films from electroless deposition ... 30
2.6 Leaks in composite Pd and Pd alloys membranes ... 32

3 Experimental set-up and procedures 36

3.1 Composite Pd membranes synthesis ... 36
3.1.1 Porous metal supports 36
3.1.2 Grading porous metal supports 38
3.1.3 Support activation 41
3.1.4 Pd plating solution 42
3.1.5 Pd deposition on activated substrates 43
3.2 The determination of H_2 permeance in composite Pd membranes ... 45
3.2.1 H_2 permeation set-up 45
3.2.2 Typical characterization procedure for a composite Pd membrane 47
3.2.3 The determination of H_2 permeance 49
3.2.4 Determination of the activation energy for H_2 permeance 50
3.3 Leaks in composite Pd membranes ... 51
3.3.1 Leak measurements and ideal separation factor 51
3.3.2 Leak distribution along the membrane length 53
3.4 Microstructure characterization methods ... 55
3.4.1 Scanning Electron Microscope (SEM) 55
3.4.2 X-ray diffraction (XRD) techniques 56
3.4.2.1 Time resolved phase transformations, High Temperature X-Ray Diffraction 57

4 H_2 permeation through Pd films 60

4.1 Introduction 60
4.2 Results and discussion 63
4.2.1 H_2 concentration in Pd: n(H/Pd) 63
4.2.2 The permeation mechanism of H_2 through Pd foils 67
4.2.3 The H_2 permeability of clean Pd 70

5 H_2 permeation through composite Pd membranes 74

5.1 Introduction 74
5.2 Theory 77
5.2.1 The model of mass transfer within the porous support 77
5.2.2 The leak model 82
5.3 Experimental 86
5.4 Results and discussion 88
5.4.1 The relevance of the n-exponent in this work 88
5.4.2 The effects of leaks on H_2 flux 93
5.4.3 The effects of mass transfer resistance in the support on H_2 flux 99
5.4.3.1 Modeling the H_2 mass transfer within the porous metal support 99
5.4.3.2 The prediction of mass transfer resistance in composite Pd membranes 105
5.4.4 Effect of Pd catalytic surface activity on H_2 flux 113
5.4.5 The activation energy for H_2 permeation in fresh composite Pd membranes 120
5.4.5.1 The Ep in fresh composite Pd membranes 120
5.4.5.2 Activation energy measured at low temperatures in composite Pd membranes 130
5.5 Conclusions 132

6 Engineering substrate surface for the synthesis of ultra-thin composite Pd membranes 133

6.1 Introduction 133
6.2 Experimental 135
6.2.1 Membranes considered in this chapter 135
6.3 Results and discussion 139
6.3.1 The structure of composite Pd-graded support membranes 139
6.3.1.1 Thickness and structure of the grade layer 139
6.3.1.2 Composite Pd membrane structure on "graded" supports 143
6.3.1.3 Effect of support quality on membrane thickness 145
6.3.2 H_2 permeance, selectivity and long-term stability of composite Pd graded-support membranes 149
6.3.2.1 The H_2 permeance of composite Pd-graded supports membranes 149
6.3.2.2 The selectivity of composite Pd graded-support membranes 157
6.3.2.3 Long term stability of composite Pd graded PH membranes 159
6.3.3 The grade layer as a barrier against intermetallic diffusion 162
6.3.3.1 The H_2 flux stability at high temperatures (>500ºC) of membrane C01-F08 162
6.3.3.2 The grade layer as intermetallic diffusion barrier 164
6.4 Conclusions 169

7 Synthesis of composite Pd-Cu membranes on engineered substrate surface 170

7.1 Introduction 170
7.2 Theory 172
7.2.1 The study of metal transformations with XRD 172
7.3 Experimental 174
7.3.1 XRD sample preparation 174
7.3.2 The preparation of a composite Pd-Cu membrane, Ma-41 176
7.4 Results and discussion 179

7.4.1 The inter-diffusion of Pd-Cu bi-layers *179*
7.4.2 The nucleation and growth of the β phase *193*
7.4.3 H_2 permeation through a composite Pd-Cu membrane *203*
7.5 Conclusions 209

8 The intermetallic diffusion mechanism in composite Pd membranes 210

8.1 Introduction 210
8.2 Experimental 211
8.3 Results and discussion 212
8.3.1 The oxidation of porous metal supports *212*
8.3.1.1 Oxide structure upon heating 212
8.3.1.2 Oxide stability in reducing atmosphere 217
8.3.2 Effect of intermetallic diffusion on H_2 permeance *224*
8.3.2.1 Effect on H_2 permeance 224
8.3.2.2 Intermetallic diffusion effect on activation energy for H_2 permeation 230
8.3.3 Intermetallic diffusion mechanism *237*
8.4 Conclusions 243

9 Effects of stress relaxation on the microstructure of fresh Pd thin films 245

9.1 Introduction 245
9.2 Stress theory 246
9.2.1 Thermal stresses *246*
9.2.2 H_2 stresses *247*
9.2.3 Stresses in a composite Pd/substrate structure *248*
9.3 Experimental 249
9.3.1 The preparation of samples *249*
9.3.2 X-ray diffraction procedures *251*
9.3.2.1 X-ray diffractometers 251
9.3.2.2 Microstrains-size separation: the Williamson-Hall method 251
9.3.2.3 Stress measurement: lattice strain Vs. $Sin^2\psi$ method 254
9.4 Results and discussion 255
9.4.1 Microstructure of a fresh electroless plated thin Pd film *255*
9.4.1.1 The morphology of fresh electroless Pd deposits 255
9.4.1.2 Initial Pd grain size, microstrains and "intrinsic" stresses 257
9.4.2 Pd microstructure changes with temperature *261*
9.4.2.1 Morphology changes with temperature 261
9.4.2.2 Grain growth and microstrains release with temperature 263
9.4.2.3 "Intrinsic" and "extrinsic" stresses release with temperature 268
9.4.3 "Extrinsic" stresses upon H_2 loading *272*
9.4.3.1 The determination of n (H/Pd) at T and P 272
9.4.3.2 The presence of compressive stresses upon H_2 loading 276
9.4.4 Estimation of stresses during membrane characterization *283*
9.4.5 The effect of atmosphere cycling *286*
9.4.6 Stress measurements in Pd-Cu –PH composite structures *288*
9.5 Conclusions 290

10 Leak growth mechanism in composite Pd membranes 292

10.1 Introduction 292
10.2 Experimental 293
10.2.1 Membrane preparation *293*
10.2.2 Membrane characterization procedures *293*
10.2.3 The activation energy for the rate of increase of leaks in composite Pd membranes *295*

10.3 Results and discussion 297
10.3.1 Pinhole size, pinhole formation *297*
10.3.1.1 Size characterization of pinholes 297
10.3.1.2 The formation of pinholes at high temperatures 303
10.3.1.3 The formation and growth of pinholes 305
10.3.1.4 Distribution of defects in composite Pd membranes 311
10.3.2 Kinetics of leak increase in H_2 atmosphere *311*
10.3.3 Leak growth in He atmosphere *318*
10.3.4 Leaks in Pd-Cu membranes: the case of Ma-41 *321*
10.3.5 The formation of leaks in composite Pd membranes prepared by the electroless deposition technique *323*
10.4 Conclusions 327

11 Conclusions 328

12 Recommendations 331

References 333
Nomenclature 347
Appendix A 349

List of figures

Figure 2-1 *Pd-H phase diagram (Shu et al., 1991). Data from Frieske and Wicke (1973). Inset data from Wicke and Nersnt (1964)* *10*

Figure 2-2 *H_2 flux ratio of Pd-Au, Pd-Ce and Pd-Y alloy* *15*

Figure 2-3 *H_2 permeance ratio of Pd-Ag, Pd-Au, Pd-Pt and Pd-Rh measured by Gryaznov (2000)* *16*

Figure 3-1 *(a) PSS, PH or Al_2O_3 plate. (b) Assembly of a blind cap, porous metal tube and non-porous metal tube* *37*

Figure 3-2 *H_2 permeation set-up* *46*

Figure 3-3 *"Rising water test" apparatus (Shell International Exploration and Production, Inc.)* *54*

Figure 3-4 *Temperature calibration curve when using a surround heater.* *59*

Figure 4-1 *$P^{0.5}$ vs. n(H/Pd) data from Gillespie and Galstaun (1936). The experimental data were fitted with a 4^{th} order polynomial function (solid lines)* *64*

Figure 4-2 *n-exponent as a function of maximum pressure for the 250, 290 and 310ºC isotherms* *66*

Figure 4-3 *H_2 permeation through a freestanding Pd film* *68*

Figure 4-4 *Pd H_2 permeability vs. 1/T for all references in Table 4-1* *72*

Figure 4-5 *Ln(H_2 permeability) vs. 1/T for all references in Table 4-1* *73*

Figure 5-1 *Scheme of a composite Pd-porous substrate structure.* *78*

Figure 5-2 *He permeance vs. P_{ave} for the graded support of C01-F11a/11b membranes* *80*

Figure 5-3 *The diffusion of H through Pd lattice ("solution diffusion") and the diffusion of H_2 through defects* *83*

Figure 5-4 *Calculated J_{H2} as function of ($P^{0.5}$-$P^{0.5}{}_0$) with r=0 and selectivity =40 (open circles) and selectivity =∞ (dashed line).* *87*

Figure 5-5 *H_2 flux and residuals as a function of $P^{0.5}$-$P^{0.5}{}_0$ at 300ºC for membrane C01-F03.* *89*

Figure 5-6 *Ln(F_n), Ln($F_{0.5}$) and n-exponent for membrane C01-F03 as a function of 1/T.* *91*

Figure 5-7 *(a) F_n vs. selectivity (b) n-exponent vs. selectivity for different r ratios* *95*

Figure 5-8 $F_{0.5}$ *vs. selectivity for different values of r* *97*

Figure 5-9 *Selectivity and n-exponent vs. temperature for C02-F01 and C02-F03 membranes* *98*

Figure 5-10 *n-exponent as a function of selectivity for C02-F01 and C02-F03 membranes* *100*

Figure 5-11 *(a) Calculated and experimental* H_2 *permeance* $F_{0.5}$*. (b) Calculated and experimental activation energy based on* $F_{0.5}$ *values (250-500ºC)* *103*

Figure 5-12 *Calculated and experimental n-exponents* *104*

Figure 5-13 *Calculated and experimental Ep changes with temperature* *106*

Figure 5-14 *Calculated n-exponent and* $F_{0.5\ composite}/F_{0.5\ foil}$ *at 500ºC as a function of* ξ_{250}*. The experimental n-exponents determined at 500ºC for membranes C01-F03/5/11b are also plotted* *109*

Figure 5-15 *Calculated* $Ep_{(450\text{-}500)}$ *as a function of* ξ_{250}*. The experimental* $Ep_{(450\text{-}500)}$ *for membranes C01-F11b and Ma-32/32b/34b/42 are plotted.* *112*

Figure 5-16 *n-exponent as a function of temperature for membranes C01-F03 and C01-F05.* *114*

Figure 5-17 *(a) Cross-section of membrane C01-F05. (b) Surface morphology of membrane C01-F05.* *116*

Figure 5-18 *Cross-section (a) and surface analysis (b) of membrane C01-F11 after* H_2 *characterization.* *118*

Figure 5-19 *n-exponent as a function of temperature for membranes C01-F05, C01-F11a and C01-F11b. n-exponents due to pressure effects and the calculated n-exponents for C01-F11b due to mass transfer effect (Figure 5-12) were also added for comparison purposes.* *119*

Figure 5-20 F_{H2} *permeance as a function of time at different temperatures C01-F03* *122*

Figure 5-21 $Ln(F_{0.5})$ *as a function of 1/T for membrane C01-F03* *122*

Figure 5-22 *Temperature change between 300 and 350ºC of membrane Ma-41* *124*

Figure 5-23 H_2 *permeance,* F_{H2}*, as a function of time during the 250-300ºC temperature change in Ma-41* *125*

Figure 5-24 $Ln(F_{0.5})$ *and* $Ln(F_{H2})$ *vs. 1/T for membranes C02-F01.* *127*

Figure 5-25 $Ln(F_{0.5})$ *and* $Ln(F_{H2})$ *vs. 1/T for membranes C01-F05.* *129*

Figure 6-1 *Surface of Ma-41 and Ma-42 composite Pd-based membranes.* *140*

Figure 6-2 *Structure within a pore achieved by sequential deposition of coarse, fine and very fine pre-activated powders.* *142*

Figure 6-3 *(a) Thin Pd layer (14μm) of C01-F09 membranes. (b) Thin Pd layer of (6-8μm) of Ma-34b membrane.* *144*

Figure 6-4 *(a) SEM micrograph of membrane C01-F09. (b) SEM micrograph of membrane C01-F03. Mag: 1000X* *146*

Figure 6-5 *He permeance vs. Pd thickness for C01-F03/5/7 (PSS supports), C01-F08/9/11 (graded PSS supports) and Ma-32/34/42 (graded PH supports)* *148*

Figure 6-6 *H_2 permeance vs. time at 250ºC for membrane C01-F09.* *150*

Figure 6-7 *Arrhenius plot of H_2 permeance, $F_{0.5}$, for composite Pd membranes prepared on non graded supports (circles) and graded supports (squares)* *152*

Figure 6-8 *Arrhenius plot of H_2 permeability for composite Pd membranes prepared on non graded supports (circles) and graded supports (squares)* *153*

Figure 6-9 *Comparison of H_2 permeance for membranes C01-F09 Ma-32/34 and Ma-42 with recent works listed in Table 6-2* *156*

Figure 6-10 *Ideal selectivity of some membranes prepared on graded supports as a function of temperature* *158*

Figure 6-11 *Long-term H_2 permeance stability at 500ºC for membrane Ma-32b* *160*

Figure 6-12 *Selectivity, H_2 permeance and He leak rate as a function of time at 500ºC for Ma-32b* *161*

Figure 6-13 *H_2 permeance as a function of time for membrane C01-F08 at 500, 550 and 600ºC* *163*

Figure 6-14 *Selectivity (H_2/He), H_2 permeance and He leak for membrane C01-F08 at 500, 550 and 600ºC* *163*

Figure 6-15 *Sections of C01-F09 heated at (a) 400ºC, (b) 500ºC and (c) 600ºC. Mag:2000X* *166*

Figure 6-16 *Composition analysis across the grade layer for the sample heated at 500ºC in H_2.* *167*

Figure 6-17 *Composition analysis across the grade layer for the sample heated at 600ºC in H_2 (a) SEM micrograph (b) Elemental analysis along arrow.* *168*

Figure 7-1 *fcc → bcc ordering transformation in PdCu alloys* *173*

Figure 7-2 *Ma-41 composite Pd-Cu membrane* *177*

Figure 7-3 *Ma-41 composite Pd-Cu membrane* *178*

Figure 7-4 *Phase changes as a function of time in sample n1 (650ºC in He)* *180*

Figure 7-5 *(a) left. XRD pattern collection of sample Pd-Cu-2 as a function of time. (650ºC in He). (b) right. XRD pattern collection while cooling from 650ºC to 300ºC. Nucleation of the β phase occurred at a temperature above 525ºC.* *182*

Figure 7-6 *XRD patterns of sample Pd-Cu-2 face 1, mainly β phase, and face 2 mainly α phase* *184*

Figure 7-7 *Elemental composition across the thickness of sample Pd-Cu-2 after heat-treatment for face 1 and face 2. The dashed line represents the penetration of X-rays at an angle of 2θ=40°* *184*

Figure 7-8 *XRD pattern collection of sample Pd-Cu-3 during heat-treatment. Part of the pattern for the homogenization process was eliminated in the 3D spectra collection.* *186*

Figure 7-9 *XRD patterns of sample Pd-Cu-3 face 1 and 2* *188*

Figure 7-10 *Elemental composition across the thickness of sample Pd-Cu-2 after heat-treatment for face 1 and face 2. The dashed lined represents the penetration of X-rays at an angle of 2θ=40°* *188*

Figure 7-11 *SEM picture of sample Pd-Cu-1 (a), sample Pd-Cu-2 (b) and sample Pd-Cu-3 (c) after heat-treatment* *190*

Figure 7-12 *(a) SEM micrograph (b) Composition profile of different elements along the arrow in by EDX line scan.* *192*

Figure 7-13 *X_β as a function of time at different temperatures after quenching from 650ºC* *195*

Figure 7-14 *phase transformation path at different times t=0 sec and t=10 min* *196*

Figure 7-15 *(a) fcc → bcc ordering transformation in the 0-200 sec. time range. (b) ordering transformation in the 0-3600 sec time range* *198*

Figure 7-16 *(a) Avrami model (b) quadratic model* *199*

Figure 7-17 *Ln (rate t=0 sec) and Ln (rate 1000-3000 sec) as a function of 1/T* *201*

Figure 7-18 *Phase transformation path at different times t=0 sec, t=10 min* *202*

Figure 7-19 *Long term H_2 stability for Ma-41 membrane.* *203*

Figure 7-20 *H_2 flux at 250-450ºC for Ma-41 membrane as function of Sieverts' driving force. Numbers beside experimental lines are the H_2 permeance $F_{0.5}$.* *205*

Figure 7-21 *Arrhenius plot for membrane Ma-41. (open circles) permeance values $F_{0.5}$ from flux data in Figure 7-20.* *206*

Figure 7-22 *Activation energy for H_2 permeation for each temperature change.* *207*

Figure 7-23 *Activation energy for H_2 permeation in PdCu alloys as a function of Cu content.* *208*

Figure 8-1 *(a) SEM micrograph of the Pd-600ºC oxidized PSS interface. (b) Elemental composition across the Pd-oxidized PSS interface.* *214*

Figure 8-2 *XRD spectra of PSS (blue) and PH (green) oxidized at 900ºC for 12 hr. (a) low 2θ range, (b) medium 2θ range and (c) high 2θ range. The reference XRD peaks of Fe_2O_3 (red dashed lines), Cr_2O_3 (green dashed lines) and $NiCrO_3$ (orange dashed lines) are also plotted for peak matching.* *216*

Figure 8-3 *(a) SEM photograph of the Pd-oxidized PSS interface after heat-treatment at 400ºC in H_2 (b) Fe concentration across the steel-Pd interface for the sample*

annealed at 400ºC in H_2 for 48 hr at 6 different locations in the sample (line-scans 1-6). One of the scans (line-scan 1) of the sample at 300ºC was added for comparison. 218

Figure 8-4 (a) SEM photograph of the Pd-oxidized PSS interface after heat-treatment at 500ºC in H_2 (b) Fe concentration profile of samples from C01-F06 annealed at 300ºC, 400ºC and 500ºC under H_2 atmosphere. 220

Figure 8-5 (a) SEM photograph of the Pd-oxidized PSS interface after heat-treatment at 600ºC in H_2 (b) Fe, Pd, Cr and Ni concentration profile across the interface. 221

Figure 8-6 (a) Cross-section of Ma-34b after heat-treatment at 600ºC in H_2 atmosphere. (b) Elemental composition across the Pd-Oxidized PH interface. 223

Figure 8-7 H_2 flux/H_2 $flux_0$ as a function of time for all temperatures membrane C01-F03, was tested....225

Figure 8-8 H_2 flux/H_2 $flux_0$ vs. time for membrane C01-F04....226

Figure 8-9 H_2 flux/H_2 $flux_0$ vs. time for membrane C01-F07....227

Figure 8-10 H_2 flux loss at different temperatures as a function of time for membrane Ma-42....229

Figure 8-11 Activation energy for H_2 permeation vs. temperature change for membrane C01-F05. 232

Figure 8-12 (a) Cross-section of C01-F05 after heat-treatment at 700ºC in H_2 atmosphere for 1 hr. (b) Elemental composition across the Pd-Oxidized PSS interface....234

Figure 8-13 Activation energy of H_2 permeation, F_{H2}, determined in several temperature ranges for membranes C01-F03, C01-F05, C01-F07, Ma-32, Ma-32b and Ma-34b....235

Figure 8-14 H_2 flux loss as a function of time at (a) 350, 400, 450 and 500ºC and (b) 500, 550, 600 and 650ºC for C01-F05 membrane. 238

Figure 8-15 Ln(H_2 flux loss rate) as a function of 1/T for C01-F03/4/5/7 and Ma-42 membranes....239

Figure 8-16 Composite image (secondary electron and backscatter of C01-F03 membrane cross-section at (a) low magnification and (b) high magnification of the same area. (Pictures taken by Larry Walker at the html, ORNL, TN) 242

Figure 9-1 Surface structure of sample PSS-1a. (a) mag: 1kX, Pd "super structure" (b) mag: 5kX, Pd clusters and (c) mag: 10kX domains of crystallites in a Pd clusters. Red squares represent the area of the next picture. 256

Figure 9-2 (a) Williamson-Hall plot of PH-1a sample. (b) Strain-$\sin^2\psi$ plot for the same Pd coating. Data taken at 20ºC....258

Figure 9-3 surface pictures of PSS-1a (a) mag.: 1kX, (c) mag.: 5kX and (e) mag.: 10kX. Surface microstructure of PSS-2a (upon heating at 500ºC for 48 hr) is shown at (b) mag.: 1kX, (d) mag.: 5kX and (f) mag.: 5kX. mag1KX, scale bar: 20 μm, mag 5KX scale bar: 5 μm and mag 10KX scale bar:2.5 μm....262

Figure 9-4 *Pd-α -Al_2O_3 deposits annealed in H_2 at (a) 300 (Al_2O_3-3a), (b) 400 (Al_2O_3-4a), (c) 500 (Al_2O_3-5a) and (d) 600ºC (Al_2O_3-6a) for 48 hr (Mag 5000)* 264

Figure 9-5 *Strain-size separation for PH-1a at different temperatures. Letters A and B correspond to the scan at room temperature before high temperatures (A) and after high temperatures exposure treatment (B).* 265

Figure 9-6 *Microstrains release in He atmosphere in sample Al_2O_3-1a as a function of temperature. Heating rate 3ºC/min.* 267

Figure 9-7 *Microstrains release as a function time for sample Al_2O_3-2a in H_2 atmosphere at 200, 300, 400 and 500ºC.* 267

Figure 9-8 *Stress release in sample PH-1a as a function of temperature* 269

Figure 9-9 *Stress in thin Pd films as a function of temperature. (◇) PH-1b, (□) PH-2a and (△) PH-3a.* 271

Figure 9-10 *Pd-H system in the high pressure and moderate temperature region. The blue dashed line represents the H_2 content (mol H/mol Pd) at 243ºC and an absolute pressure of 5 bar.* 273

Figure 9-11 *$P^{0.5}$ vs. n(H/Pd) at 30 and 160ºC. Experimental data from (Gillespie and Hall, 1926).* 275

Figure 9-12 *Arrhenius plot for $K(=P^{0.5}/n(H/Pd))$ derived from experimental data reported by (Gillespie and Hall, 1926), (Gillespie and Galstaun, 1936) and (Wicke and Nernst, 1964). Temperature range: 0-300ºC* 275

Figure 9-13 *Comparison in H_2 concentration n from isotherms and using Equation (9-15)* 277

Figure 9-14 *Pd-H system in the low pressure and low temperature region. The red line represents the $\alpha/(\alpha+\beta)$ boundary. The blue line represents the H_2 loading (mol H/mol Pd) at 60ºC and an absolute H_2 pressure of 0.06 bars. The green line represents the H_2 loading (mol H/mol Pd) at 50ºC and an absolute H_2 pressure of 0.04 bar.* 279

Figure 9-15 *Pd lattice expansion due to H_2 uptake and temperature in sample PH-1c* 280

Figure 9-16 *Lattice increase due to interstitial H_2 for sample PH-1c* 280

Figure 9-17 *Stresses arisen in the Pd thin film due to H_2 uptake* 282

Figure 9-18 *H_2 stress as a function H_2 content n(H/Pd)* 282

Figure 9-19 *Total stress calculations for a Pd composite membrane as a function of pressure difference at 250, 300, 400 and 500ºC. Solid lines at 250 and 300C represent stress calculation using the actual isotherms at 250 and 300C (Gillespie and Galstaun (1936) for the determination of n (H/Pd). Dashed lines represent stress calculations using Equation 5.19 for the determination of n (H/Pd)* 284

Figure 9-20 *Microstrains in He and H_2 atmosphere for sample PH-4a pre-annealed in He at 400ºC for one hour* 287

Figure 9-21 *Thermal stresses as a function of temperature for the β phase (open circles) and the α phase (open diamonds)* *289*

Figure 10-1 *Schematic H_2 vs. time plot for a composite Pd membrane.* *297*

Figure 10-2 *He and Ar permeance of Ma-41 as a function of average pressure across the membrane.* *299*

Figure 10-3 *β/α ratio as a function of $M^{0.5}/\eta$ for He and Ar.* *301*

Figure 10-4 *Ma-32c surface morphology after annealing in H_2 at (a) 500, (b) 550, (c) 600 and (d) 650ºC for 48 hr (Mag 1500)* *304*

Figure 10-5 *He permeance vs. average pressure at 500ºC at time t=0, 200, 400 and 550 hr and t=60 hr at 550ºC.* *306*

Figure 10-6 *He leak rate vs. time at 450ºC and 500ºC for membrane Ma-41. The total pinhole area (ε_α·S) as function of time at 500ºC and 550ºC was also plotted.* *308*

Figure 10-7 *Pinhole diameter and number of pinholes as a function of time at 450ºC and 500ºC.* *308*

Figure 10-8 *He leak rate vs. time at 500ºC and 550ºC for membrane Ma-34b. The total pinhole area (ε_α·S) as function of time at 500ºC and 550ºC was also plotted.* *310*

Figure 10-9 *Pinhole diameter and number of pinhole as a function of time at 450ºC and 500ºC.* *310*

Figure 10-10 *He leak as a function of water level for membrane Ma-32b/32c. The "0" mark corresponds to the lower weld and the "15" mark corresponds to the upper weld.* *312*

Figure 10-11 *He leak of membranes C01-F11/11b and membrane Ma-41 and Ma-42 as a function of temperature.* *313*

Figure 10-12 *He leak rate increase in H_2 atmosphere at 450, 500 and 550ºC for membrane Ma-34b.* *315*

Figure 10-13 *Arrhenius plot for membranes C01-F11a/11b and membranes Ma-32b, Ma-34b, Ma-41 and Ma-42. The activation energy was estimated in the 450-550ºC temperature range.* *317*

Figure 10-14 *He leak increase at 500ºC of membrane Ma-34b in He atmosphere (circles) and in H_2 atmosphere (filled circles). The He leak increase of membrane Ma-32c at 500ºC in H_2 atmosphere was also plotted for comparison purposes.* *320*

Figure 10-15 *Ideal selectivity (H_2/He) and He leak (sccm) as a function of time exhibited by the Pd-6.8wt% Cu membrane at 450ºC in H_2 atmosphere* *322*

Figure 10-16 *Jump into a vacant site. (a) Atoms 1 and 2 need to stretch. (b) The four dashed atoms need to stretch in the fcc cell (Porter and Easterling, 1981).* *325*

Figure 10-17 *Mathematical simulation of (a) coherent sintering and (b) incoherent sintering (Skorokhod, 2003)* *326*

List of tables

Table 2.1 *Pd plating bath and plating conditions commonly reported in the literature* *23*

Table 3-1 *Pd plating bath and deposition conditions for membrane preparation* *42*

Table 3-2 *List of all membranes studied in this work* *44*

Table 4-1 *H_2 permeability for Pd measured in Pd foils in previous works* *70*

Table 5-1 *Support characteristics, Pd film thickness, ξ_{250} parameter and $Ep_{450-500}$ for all membranes in this chapter* *108*

Table 5-2 *$Ep_{(250-300)}$ and $Ep_{(300-350)}$ for C01-F03/5/7/8/11/11b membranes* *131*

Table 6-1 *Al_2O_3 powders and binding conditions for the grading of C01-F08/9/11 and Ma-32/34/41/42* *137*

Table 6-2 *Characteristics of all composite Pd membranes studied in this work.* *138*

Table 6-3 *Percentage loss of the initial He permeance of the bare porous metal support after grading step.* *141*

Table 6-4 *Characteristics recent composite Pd membranes reported in the literature.* *155*

Table 7-1 *Chemical composition of Pd and Cu plating bath* *176*

Table 7-2 *List of Pd-Cu samples used in this Chapter* *176*

Table 8-1 *Characteristics of membranes studied in this chapter.* *212*

Table 8-2 *Temperature at which H_2 permeance loss was first recorded for several membranes.* *230*

Table 8-3 *Activation energy for H_2 flux loss rate for all membranes in Figure 8-15 in the low (T<500ºC) and high (T>500ºC) temperature range* *240*

Table 9-1 *List of samples studied in this chapter.* *250*

Table 10-1 *Characteristics of composite Pd membranes considered in this chapter* *294*

Table 10-2 *He leak and selectivity of membranes considered in this chapter* *302*

1 Introduction

The fossil energy reserves, mostly oil and methane, that we have been burning for years are expected to reach a production peak in the middle of the 21st century (Bartlett, 2000; Campbell and Laherrere, 1998; Duncan and Youngquist, 1999; Edwards, 1997; IEA, 1997). When the oil and methane production peaks, it will initially perturb prices, changing the world economy in a drastic manner. Coal reserves are still important worldwide. For instance, the United States of America's coal reserves are thought to last for 250 years, although we all know, burning coal will certainly lead, even with the cleanest coal technologies, to large amounts of CO_2 released to the atmosphere.

Soon, a new source of energy will have to be found. There exists the alternative to synthetically manufacture fuels via coal gasification followed by Fischer-Trops synthesis to produce highly branched hydrocarbons. Although gasification may be coupled with very attractive carbon sequestration technologies, the overall process is not secure enough. Carbon sequestration consists of trapping the CO_2 by pumping it in liquid form into deep oceans or by pressurizing old oil reservoirs (tertiary oil recover) with it. Yet, questions on the fate of the trapped CO_2 after years still remain. To guarantee the safe continuity of our civilization and development, it is imperative to decrease the fast rate of burning fossil fuels and coal, in order to limit the amount of CO_2 released into the atmosphere. Therefore, both for urgent environmental safety and acknowledging the economic

impact of a diminishing reserve of fossil fuels a new and clean source of energy needs to be found.

One of the most attractive alternatives for energy production is the oxidation of H_2 with air. This chemical reaction releases large amounts of energy with only H_2O as by-product. Therefore H_2 would be one of the cleanest sources of energy. In fact, H_2 is an energy carrier and not an energy source. Indeed, H_2 is not naturally available as oil but has to be produced by splitting the H-C bonds in hydrocarbons or the H-O bonds in water or alcohols, which requires large amounts of energy.

H_2 is nowadays produced at low cost mainly from the steam reforming of methane. H_2 is essentially used (two thirds of the world production) for the production of ammonia, which is the main chemical for the synthesis of fertilizers. Secondly, H_2 is used in the petrochemical industry for the refining of sour crude oils and in the semiconductor industry during sputtering processes. Finally, a small amount is used as chemical for the hydrogenation of edible oils and a very small amount as fuel in the rocket industry. The first use of H_2 is particularly important, since fertilizers are a crucial component of today's large scale agricultural industry, and the absence of it could result in a widespread hunger. Hence, the sustainability of the 7 billion humans on Earth is indirectly related to the production of H_2, which is still ensured by the presence of CH_4.

If a shortage of fossil fuels exists, humankind may need to choose nuclear energy to solve the global energy and food problems. Indeed, nuclear energy can be used to produce electricity, which can be used for the production of H_2. H_2 can be used for the production of fertilizers and as energy carrier in transportation vehicles by means of the fuel cells. Nuclear energy is very safe and clean although waste management poses seri-

ous problems. Moreover, the sad accident occurred in Chernobyl and all the terrible consequences that people are still witnessing in the disaster area are still in our minds. Humankind is indeed reluctant to use nuclear energy for all its power needs. Hoping that one day we will be able to capture solar, wind and other unlimited energy sources with economically viable technologies to break water molecules by electrolysis and produce H_2 for food and energy needs, the safe (compared to nuclear) and short-term solution for H_2 production is the improvement of the steam reforming of hydrocarbons process to make it more economical and environmental friendly. H_2 production from steam reforming of hydrocarbons coupled with membrane technology is indeed the preliminary step towards a carbon free energy economy.

A more efficient process to convert fossil fuels into H_2 is by using a Pd based membrane reactor, where the steam reforming reaction and the separation process (with a Pd based composite membrane) are carried out in the same vessel. Di-atomic hydrogen, H_2, has the unique ability to dissociate on the catalytic surface of Pd to form H atoms that can readily diffuse through the Pd bulk. Since no other gas molecule can pass through the Pd or Pd-alloy films, an infinite selectivity for H_2 separation is possible. Therefore, in theory, composite Pd and Pd-alloy membranes are infinitely selective to H_2. Also, Pd membranes are of preference to extract the H_2 from the reactant mixture due to their high mechanical and thermal stability. Combining the reaction and the separation in the same unit operation allows the use of lower temperature (500ºC), which represents a saving in energy, higher yields due to the removing of H_2 during reaction, pure H_2 and high pressure CO_2 that would be suitable for sequestration.

The prospect of higher yields H_2 production has sparked academic and industrial interests. The production of H_2 from hydrocarbons steam reforming in Pd based membrane reactors has been proven to work in laboratory scale reactors. Research on hydrocarbon steam reforming in Pd based membrane reactors has been carried out in Taiwan (Lin et al., 1998; Lin and Rei, 2000, 2001), Japan (Itoh et al., 2002; Itoh et al., 2003; Kikuchi, 2000; Kikuchi et al., 2000; Shirasaki et al., 1997) and United States of America (Matzakos et al., 2003; Wellington et al., 2003). Mathematical models on Pd-based membrane reactors have also been developed (Marigliano et al., 2003). Steam reforming and/or partial oxidation of carbonaceous compounds were carried out in membrane reactors using essentially Pd (Galuszka et al., 1998; Kikuchi, 2000; Lin and Rei, 2001), Pd-Ag alloys (Wieland et al., 2002), and PdCu alloys (Han et al., 2002; Wieland et al., 2002) composite membranes or foils for H_2 separation.

Pd alloys are preferred over pure Pd since Pd undergoes a phase transformation (α to β) when exposed to H_2 at temperatures lower than 300°C and high H_2 pressures. This phenomenon, called 'H_2 embrittlement', is due to the lattice parameter of the β phase being larger than that of the α phase. Indeed, stresses are induced during the nucleation of the β phase leading to distortions in the dense composite membrane or foil. Therefore, multiple H_2 absorption/desorption cycles at room temperature induce series of α to β and β to α transformations leading to the deformation or cracking of the Pd membrane. Alloying Pd with other metals such as Au, Ag, Cu, Fe, Ce and Y decreases the critical temperature above which no α to β transformation occurs. Thus, Pd alloys can undergo H_2 absorption/desorption cycles at lower temperatures than 300°C without failure due to H_2 embrittlement. Moreover, some alloys have even greater H_2 permeability than pure

Pd. Examples of high H_2 permeability alloys are: $Pd_{77}Ag_{23}$[1], $Pd_{60}Cu_{40}$, $Pd_{90}Y_{10}$, $Pd_{80}Au_{20}$ and others. Ternary alloys also showed, in special cases, greater H_2 permeability than pure Pd. Examples are: $Pd_{93.5}Ru_{0.5}In_{6.0}$ and $Pd_{80}Ag_{19}Rh_1$ having respectively a H_2 permeability of 2.8 and 2.6 the H_2 permeability of pure Pd (Gryaznov, 2000). Furthermore, some alloys such as Pd-Cu and Pd-Au showed resistance in H_2S containing feed streams, which make them very attractive for H_2 separation from coal gases.

Laboratory scale reformers include thin Pd and Pd alloy foils (cold rolled) or thin composite Pd or Pd alloy membranes (Pd deposited on a porous substrate) as H_2 separators. It is not yet clear which technology will prevail in industrial Pd based membranes steam reformers, although, due to their easy manufacturing on tubular supports, composite Pd membranes may be chosen in the future. Indeed, tubular geometry, compared to planar geometry, is generally easier to adopt for industrial applications.

High H_2 flux membranes can be achieved by depositing a thin film (<10μm) of Pd or Pd alloy on top of a porous substrate to give the necessary mechanical strength to the thin metallic layer. Vycor glass, ceramics and Porous Metals (PM) can be used as porous substrates. PM substrates have great chances to be implemented in industrial application due to their easy handling and mechanical properties. However, the main drawback of PM supports is that at high temperatures the metallic elements of the support (Fe, Ni and Cr) diffuse into the Pd layer, thereby decreasing the H_2 permeability of the composite membrane. This phenomenon, called "intermetallic diffusion" is not encountered in ceramics. Yet, ceramics supports are too brittle and difficult to connect to metal parts for industrial applications. Several methods can be used for the deposition of Pd on porous substrates,

[1] All subscripts in weight percent.

however, four methods are widely used: Chemical Vapor Deposition (CVD), sputtering, electrodeposition and electroless deposition. Electroless deposition has the advantage over the others of being inexpensive, easy to put in practice and the Pd deposits can be very uniform on complex shapes. Depositing Pd alloys with electroless or electrodeposition is a challenge. If a Pd alloy membrane is desired, the "coating and diffusion" technique is applied. This technique consists of the sequential electroless deposition of the two metals in two distinctive layers followed by heat-treatment at high temperatures. The resulting membranes show a composition gradient across the thickness unless very high temperatures are used (>650ºC). Sputtering techniques are more suited for composite Pd alloy membranes preparation.

Generally, composite Pd membranes are prepared at temperature and pressure conditions different from the ones they will be used in a membrane reactor. Moreover, fresh thin films are characterized by remaining "intrinsic" stresses and a large surface energy due to the fine-grain structure (build up of energy) that are automatically released at high temperatures. Therefore, at the reaction temperature of 500ºC, composite Pd membranes undergo a series of structural transformations that lead to several problems such as H_2 permeance loss and H_2 selectivity decrease over time.

The main objective of this research was to understand the fundamental principles involved in the synthesis, H_2 transport mechanism, mechanical and chemical stability of very-thin (<10μm) composite Pd and Pd alloy membranes prepared by the electroless deposition method on PM supports. The effects of surface roughness of the porous support on the thin Pd film thickness and the thin Pd film morphology were elucidated. The effects of gas transport properties of the porous support, H_2 diffusion through defects and

the catalytic activity of the Pd surface on the permeation mechanism of H_2 was also studied. The intermetallic diffusion phenomenon was investigated in a wide range of temperatures to understand the diffusion mechanism of Fe, Cr and Ni elements of the metal support into the Pd layer. In addition, the 'extrinsic" stresses on the Pd film due to the film/substrate mechanical interaction at high temperatures were studied. Finally, large efforts were invested in the understanding of the microstructure and microstructure changes at high temperatures of the thin Pd film constitutive of the composite Pd membrane. Specially, a detailed study on the kinetics of leak formation was undertaken.

In summary, the specific objectives were to:

(1) Understand the H_2 diffusion mechanism through composite nanocrystalline Pd membranes.

(2) Understand the effect of Pd surface catalytic activity, defects and porous support resistance on the mechanism of H_2 permeation.

(3) Understand the diffusion mechanism of the metal elements in the porous support (Fe, Cr and Ni) into the Pd layer in order to limit or inhibit the diffusion of these elements into the Pd layer.

(4) Understand how the surface roughness and morphology of the porous support affect the structure and the thickness of the dense Pd layer.

(5) Understand how the surface of porous metal supports can be modified to facilitate the formation of thin membranes.

(6) Understand how "extrinsic" and "intrinsic" stresses affect the long-term mechanical stability of the Pd thin film structure.

(7) Understand the mechanism of leak formation and leak growth in composite Pd membranes by studying the kinetics of leak growth over time at high temperatures in thin composite Pd membranes.

(8) Develop ways to avoid the formation of leaks and/or limit their growth.

2 Literature review

2.1 Pd and Pd-alloys systems

Several materials have the ability to permeate only H_2 although Pd has been the most studied system since the end of the 19th century (Graham, 1869a). The thermodynamics of the Pd-H system were studied in detail at cryogenic temperatures (Mitacek and Aston, 1963), at high pressures and high temperatures (Levine and Weale, 1960) as well as moderate temperatures and pressures (Frieske and Wicke, 1973; Gillespie and Galstaun, 1936; Gillespie and Hall, 1926; Wicke and Nernst, 1964). Figure 2-1 shows the pressure concentration isotherms (*p-n* isotherms) for the Pd-H system (Shu et al., 1991). The data plotted in Figure 2-1 were reported by Frieske and Wicke (1973) and Wicke and Nersnt (1964). In Figure 2-1, the H_2 solubility, n (=H/Pd), which is the ratio of H atoms absorbed per Pd atom is given as a function of the H_2 partial pressure, P_{H2}. The Pd-H system exhibits a miscibility gap region where two phases, α and β, both having a face centered cubic (fcc) crystalline structure, coexist at temperatures below 300°C. The miscibility gap is characterized by pressure invariance isotherms. For every isotherm, $P^{0.5}{}_{H2}$ initially increases linearly with n (see inset Figure 2-1). At n(H/Pd)=α_{max}, which is the maximum H_2 solubility in the α phase for a particular isotherm, $P^{0.5}{}_{H2}$ reaches a plateau (invariance in pressure) and the β phase, with a minimum H_2 concentration n(H/Pd)=β_{min}, nucleates.

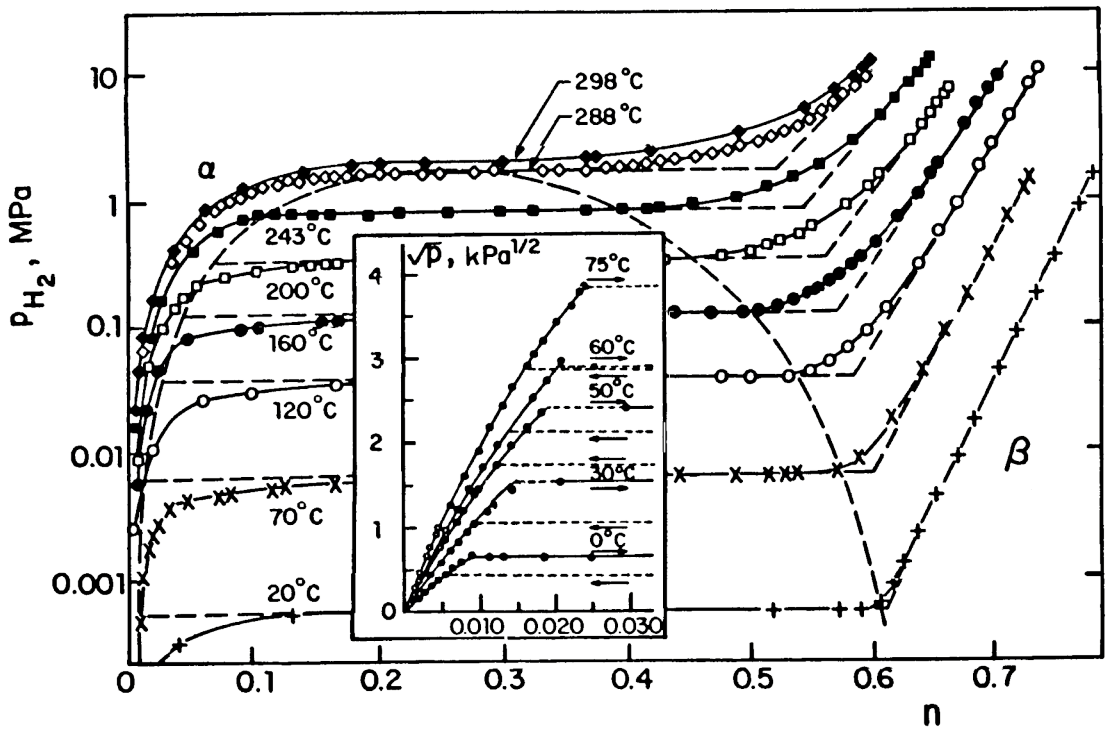

Figure 2-1 Pd-H phase diagram (Shu et al., 1991). Data from Frieske and Wicke (1973). Inset data[1] from Wicke and Nersnt (1964)

[1] In the original review by Sue et al. (1991) the y-axis values were 10, 20, 30 etc. It appeared that these numbers were mistaken and correct values are: 1, 2, 3 etc. The correction was made based on the original article by Wicke and Nernst (1964).

During the α to β transformation, the H_2 content of the α phase (α_{max}) and the H_2 content of the β phase (β_{min}) do not change, only the relative proportions of the α and the β phase does. The β phase, PdH_2, has a lattice parameter somewhat larger than that of the α phase, therefore, when the β phase nucleates within the α phase matrix, distortions appear in the metal. The modifications in shape and microstructure that occur in a Pd foil after several α→β→α transformations are denoted as "H_2 embrittlement" (Lewis, 1967). The H_2 separation properties of Pd foils that underwent several α→β→α transformations are poor due to the large numbers of microcracks. Therefore, in all H_2 purification systems based on Pd membrane technology, care is taken not to exceed the maximum H_2 concentration n(H/Pd)=α_{max} of the α phase above which the β phase nucleates. The maximum H_2 concentration n(H/Pd)=α_{max} is reached at a given H_2 pressure P_{max}, which depends on temperature according to Equation (2-1) (Gillespie and Galstaun, 1936).

$$\log(P_{max}) = 4.6018 - \frac{1877.82}{T} \qquad (2\text{-}1)$$

where P_{max} is in atm and T in K. At a temperature equal to 295.3ºC and a pressure equal to 19.87 atm a critical solution is reached (Gillespie and Galstaun, 1936) so that at temperatures above 300ºC, the α→β transformation no longer occurs. Alloying Pd with other metals decreases the temperature of the critical solution making Pd alloys less prone to H_2 embrittlement.

The Pd-Ag system is probably the most studied Pd alloy since it was found that Pd-Ag alloys absorb more H_2 than does pure Pd (Graham, 1869b). Pd-Ag alloys with more than 20 wt%[1] Ag did not show signs of distortion after thirty cycles of heating and cooling in

[1] wt% = weight percentage

H_2 atmosphere at atmospheric pressure (Hunter, 1960). The great mechanical stability of this alloy to withstand temperature cycling, when pure Pd would have distorted, was understood when *p-n(H/Pd)* absorptions isotherms at 50°C were taken for several Pd-Ag alloys and showed no pressure invariance regions (or miscibility gap) for Pd-Ag alloys having more than 20 wt% Ag (Brodowsky and Poeschel, 1965). Thus, by increasing the amount of silver, the α-β miscibility gap was depressed to lower temperatures. Even small percentages of Ag, 5 to 10 at%[1], led to the decrease of the critical temperature below which the α→β transformation occurs (Fazle Kibria and Sakamoto, 2000). In addition, the Pd-Ag alloy with 27 wt% Ag had higher H_2 permeability than pure Pd (Hunter, 1960).

The permeability coefficient, *Q*, is the product of the H_2 diffusion coefficient, *D*, and the H_2 solubility, *S*. For almost all Pd systems, *D* decreases in the presence of alloying elements and it is particularly true for Ag. However, *S* is largely increases when the Ag content is about 30 wt% Ag (Holleck, 1970; Sieverts et al., 1915). Therefore, an optimal Ag composition for the highest H_2 permeability exists between 20 and 40 wt% Ag. The highest permeability for the Pd-Ag alloys was measured for a composition of 27 wt% Ag (McKinley, 1969) and also for a composition of 23 wt% Ag (Holleck, 1970). The H_2 permeability of the $Pd_{77}Ag_{23}$ alloy is believed to reach 1.7 times the H_2 permeability of pure Pd.

Alloying Pd with Cu also decreases the critical temperature of the miscibility gap, although little work has been done on the Pd-Cu system. This is due to the fact that at the optimum Cu concentration, 40 wt% Cu, the permeability of the alloy is only 1.1 times the

[1] at% = atomic percentage

permeability of pure Pd (McKinley, 1967). The $Pd_{60}Cu_{40}$ alloy does not undergo any α to β transformation even at room temperature since its *p-n(H/Pd)* isotherm at 25°C does not show any invariance in pressure (Karpova and Tverdovskii, 1959). Therefore, Pd-Cu is one of the most robust systems available for H_2 purification. Yet, at temperatures higher than 400°C, the $Pd_{60}Cu_{40}$ alloy loses its ordered bcc structure (β phase[1]), which has a high H_2 permeability, and transforms into a disordered fcc phase (α phase[2]), which has a low permeability (Subramanian and Laughlin, 1991). The H_2 flux of the $Pd_{60}Cu_{40}$ alloy was experimentally observed to decline during the α to β phase transformation that occurred at 400ºC (McKinley, 1967). Since Pd-Cu alloys lose their high H_2 permeance structure above temperatures ranging from 400 to 600°C depending on the copper content, Pd-Cu membranes are suitable for low temperatures H_2 purification applications. Indeed, the ordered β CuPd phase has the highest H_2 permeability at low temperatures among all metal-hydrides systems. Recently, the possibility of having H_2 permeance stability of Pd-Cu alloys in atmospheres containing H_2S triggered considerable amounts of studies on the Pd-Cu alloys membrane preparation and characterization (Hoang et al., 2004; Nam and Lee, 2001; Roa et al., 2003), Pd-Cu alloy oxidation (Roa and Way, 2005) and Pd-Cu alloys permeability calculations and estimations (Kamakoti et al., 2005; Kamakoti and Sholl, 2003). More interestingly the α phase, with low H_2 permeability, appeared to be more stable than the β phase in the presence of H_2/H_2S mixtures (Morreale et al., 2004). Therefore, a compromise needs to be found between H_2S poisoning stability and H_2 permeance.

[1] Not to confuse with high H content Pd hydrides, also named β phase.
[2] Not to confuse with low H content Pd hydrides, also named α phase.

Many other metal alloys have been studied beside Pd-Ag and Pd-Cu alloys. The Pd-Au system showed higher H_2 permeabilities than pure Pd although the experimental results of different research groups differed somehow (Gryaznov, 2000; McKinley, 1967). Pd/Ce and Pd/Y alloys showed very high H_2 permeabilities and very good mechanical properties (Farr and Harris, 1973; Fort et al., 1975). The H_2 fluxes of the Pd-Au, Pd-Ce and Pd-Y systems at 350°C and 20.4 atm for 25 μm thick membranes were reviewed and are shown in Figure 2-2 (Knapton, 1977). It is important to note in this figure the large increase in H_2 flux, up to 3.7 times that of pure Pd, with small amounts of Y.

Figure 2-3 shows the Pd alloy permeance at 500ºC over the pure Pd permeance with Ag, Au, Pt and Rh alloying elements as a function of the amount of the alloying element (Gryaznov, 2000). Comparing Figure 2-2 with Figure 2-3, a large difference in H_2 permeability for the Pd-Au system can be observed between McKinley's work and Gryaznov's work. Indeed, everything being the same, Gryaznov found that the Pd-Au system, with Au compositions ranging from 5 to 20 wt%, showed H_2 permeances equal to twice the H_2 permeance of pure Pd. On the other hand, according to McKinley, the Pd-Au system, with Au composition ranging from 5 to 20 wt%, hardly reached the performances of pure Pd.

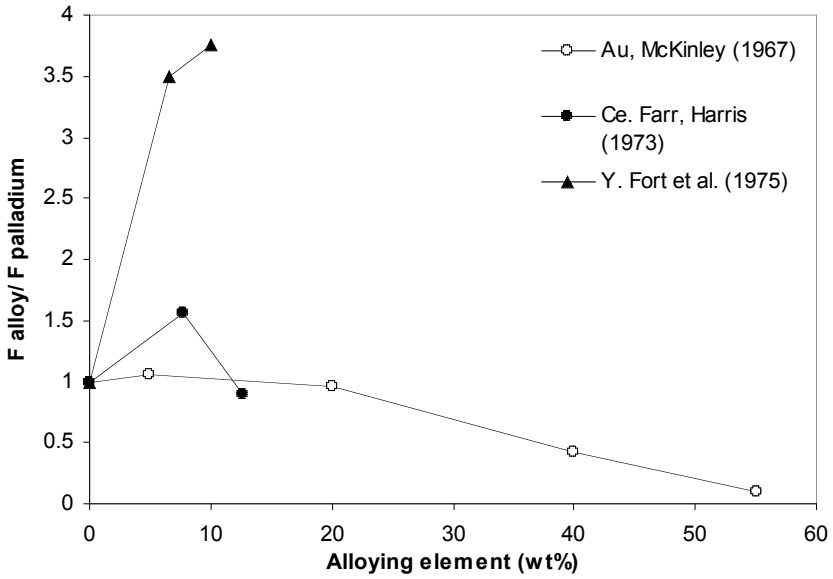

Figure 2-2 H_2 flux ratio of Pd-Au, Pd-Ce and Pd-Y alloy

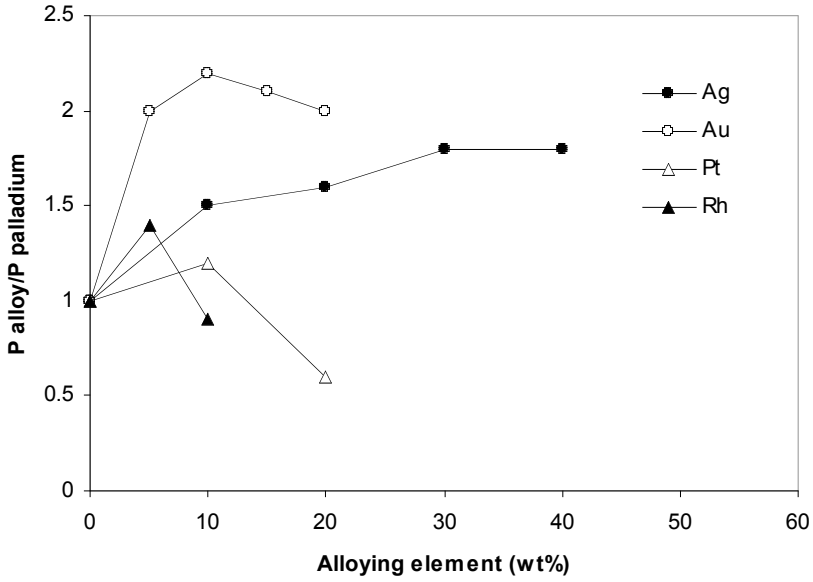

Figure 2-3 H_2 permeance ratio of Pd-Ag, Pd-Au, Pd-Pt and Pd-Rh measured by Gryaznov (2000)

Ternary alloys were also studied (Gryaznov, 2000). The $Pd_{93.5}Ru_{0.5}In_{6.0}$ showed a ratio of H_2 permeability over pure Pd of 2.8 and the $Pd_{80}Ag_{19}Rh_1$ system showed a ratio of 2.6. Since binary and ternary alloys discussed in the present section were mainly arc-melted under Ar, cooled to room temperature and rolled into thin foils, their composition was uniform and data obtained were in general very reliable.

2.2 Methods of Pd deposition onto porous substrates

The H_2 permeability of all Pd alloys described in Section 2.1 was measured with foils. Interesting works showed that wrapping a porous support with a Pd or Pd-alloy foil was technically possible, and led to very high conversion factors when used in Catalytic Membrane Reactors (CMR) (Tosti, 2003; Tosti et al., 2002; Tosti et al., 2000). However, thinner composite Pd and Pd alloy membranes can be prepared by deposition of a thinner layer than that of foils, which is usually around 20μm, on a porous substrate. Four methods are commonly used for composite Pd and Pd alloy synthesis on porous substrates. These are:

- Chemical Vapor Deposition (CVD) is the reduction or decomposition of a volatile compound of the coating material upon a heated surface. CVD allows depositing coatings of most refractory metals while other techniques are unsuccessful. CVD leads to pure and thin layers on small substrates. However the procedures are tedious and nearly impossible for industrial purposes. Metal-Organic Chemical Vapor Deposition (MOCVD) differs from CVD in that only high purity organo-metallic compounds are used. CVD was used by many researchers (Jun and Lee, 2000).

- Sputter techniques: magnetron sputtering deposition is achieved by applying a high voltage across a low-pressure gas (usually argon at about 5 mtorr) to create a "plasma," which consists of electrons and gas ions in a high-energy state. During sputtering, energized plasma ions strike a "target," composed of the desired coating material (pure Pd or a Pd alloy), and cause atoms from that target to be ejected with enough energy to travel to, and bond with, the porous substrate. A powerful magnet is used to confine the "glow discharge" plasma to the region closest to the target plate. A similar technique, Electron Beam (e-beam) evaporation can be used for Pd and Pd-alloy deposition. In e-beam evaporation the porous substrate is placed in a high vacuum chamber at a desired temperature with a crucible containing the material to be deposited. An electron beam is aimed at the material in the crucible causing it to evaporate and condense on all exposed surfaces in the vacuum chamber and substrate. Several crucibles, with different compounds (or metals), are available in the same chamber and switching crucibles leads to the evaporation and condensation of different compounds. Ion-Beam (i-beam) evaporation is essentially the same as e-beam but using argon ions instead of electrons. Magnetron sputtering, e-beam evaporation and ion beam evaporation, which are called physical vapor deposition (PVD), are generally applied when depositing alloys. The main drawback of sputtering techniques is that sputtering chambers have a confined space and coating of large supports for large scale high purity H_2 production is almost impossible. CVD and sputtering techniques offers the very attractive advantage that they allow for the support to be heated during deposi-

tion, which in turn allows for the possibility of controlling the film microstructure (Dirks, 1977; Thornton, 1974; Zhao and Xiong, 1999). The microstructure of the Pd thin film is a determinant parameter in long-term composite membrane stability, since the microstructure changes as the composite Pd membrane is exposed to reactions conditions (Roa and Way, 2005; She, 2000).

- Electrodeposition of metals involves the movement of positive metallic ions towards the cathode to be reduced and finally be incorporated in the metallic growing film. The film thickness depends on the electrolyte used, temperature, pH and mainly on current density and time. Variants of electrodeposition are vacuum electrodeposition, where vacuum is applied at the cathode, and pulsed electrodeposition where the electrical potential is varied over time (pulsed) to improve the uniformity of the deposition. Vacuum electrodeposition led to thinner and more selective films than electrodeposition (Nam and Lee, 2000; Nam et al., 1999).
- Electroless deposition is the reduction of metastable metallic salt complexes by a reducing agent on a target surface. It has been widely used for Pd membrane synthesis. This is due to the low cost, easy procedures and simplicity of the needed equipment. The advantage of the electroless deposition over the electrodeposition is that substrates do not have to be conductive and one can cover the surface of complicated shapes uniformly where electrodeposition tends to cover “hills” with a thicker layer while letting “valleys” poorly covered. The main draw back of electroless (and electrodeposition) deposition is that the deposition of alloys represents a challenge since co-deposition of two metals is

difficult. In general, when a Pd-alloy is desired, the two metals are deposited sequentially and heat-treated at high temperatures to obtain the alloy. Such process was denoted as coating and diffusion technique (Uemiya et al., 1991b; Uemiya et al., 1991c).

2.3 Electroless deposition of Pd and Pd alloys coatings

The following section describes the electroless deposition method due to its relevance to the understanding of the morphology, microstructure and properties of composite Pd membranes prepared in this study.

2.3.1 Activation of the substrate

Prior to electroless deposition, the porous substrates need to be activated. The activation process can be achieved using sequential dipping in $SnCl_2$-HCl (1 g/l, pH: 2) and $PdCl_2$-HCl (1 g/l, pH: 2) solutions. Sn^{2+} reduces Pd^{2+} by the following equation leading to the deposition of active Pd nuclei on the surface of the substrate. The size of the deposited nuclei (5.5 nm) was determined by considering the Binding Energy (BE) shift of the Pd $3d_{5/2}$ peak (Takasu et al., 1978).

$$Sn^{2+} + Pd^{2+} \rightarrow Sn^{4+} + Pd^{0}$$

This activation method has been widely used when electroless plating was applied. Moreover a wide range of substrates, including plastics and metals, can be activated. High resolution XPS scans of the Sn $3d_{5/2}$ and Pd $3d_{5/2}$ peaks were conducted after sensitizing (dip in the $SnCl_2$ solution), activation (dip in the $PdCl_2$ solution), thorough washing with DI water and finally Cu deposition of fly-ash particles (Shukla et al., 2001). Shukla et al. (2001) found that $SnCl_2$ was present on the surface just after sensitizing indicating

the good adhesion of Sn^{2+} ions on the surface of fly-ash particles. After activation, $SnCl_4$, $PdCl_2$ and Pd^0 were found on the surface confirming the reaction step leading to Pd nuclei. The DI water cleaning step led to $Sn(OH)_4$, PdO, $PdCl_2$ and Pd^0 indicating that Sn^{4+} and Cl^- ions remained on the surface even after the washing step. After the Cu deposition step, Sn^{4+} and Cl^- were neither detected on the surface of the Cu deposit nor underneath the coating using EDX analysis on a cross section of a particle. However, element composition less than 1 wt% can not be detected by EDX, therefore, traces of Sn^{4+} and Cl^- could still remain underneath the Cu coating. The absence of Cl^- and Sn^{4+} impurities after Cu plating was attributed to the dissolution of $Sn(OH)_4$ and $PdCl_2$ by the alkaline Cu plating solution.

Paglieri et al. (1999) compared the long term stability of membranes activated with the usual Sn-Pd procedure and the long term stability of membranes activated by a new activation method. The new method consisted of the deposition of $Pd(O_2CCH_3)_2$ on the surface to be plated and burnt off the organic fraction by heat treatment. They noticed that membranes activated with $Pd(O_2CCH_3)_2$ were more stable over time than those activated by Sn-Pd procedure. Therefore, they attributed the lack of long term stability showed by Pd membranes activated with Sn-Pd procedure, to Sn^{4+} impurities trapped between the palladium layer and the support. UV-light was also used to reduce $PdCl_2$ or Pd-acetate on porous substrate and avoid Sn contamination (Wu et al., 2000; Zhang et al., 1997). Pd nuclei obtain by UV-light reduction were as small as 2 nm (Lafferty et al., 1997).

A new trend in the past 10 years consisted of applying an activated layer on the support, which decreases the number of synthesis steps and the amount of raw materials.

Ceramic supports were activated with Pd(II)-modified boehmite sol gel. After calcination and reduction under H_2 at 500°C, Pd nuclei were obtained on the substrates (Li et al., 1996; Zhao et al., 1998). ZrO_2 sols were also doped with Pd nuclei, cast on Porous Stainless Steel (PSS) substrates to form a smooth activated surface for the deposition of Pd (Gao et al., 2005).

2.3.2 The chemistry of Pd deposition

A palladium plating bath includes: a palladium ion source ($PdCl_2$, $Pd(NH_3)_4Cl_2$, $Pd(NH_3)(NO_3)_2$, $Pd(NH_3)_4Br_2$), a complexant (ethylenediamine tetra acetic acid (EDTA), ethylenediamine (EDA), ammonia (NH_3)), a reducing agent (hydrazine (NH_2-NH_2), sodium hypophosphite ($NaH_2PO_2 \cdot H_2O$), Trimethylamine borane), stabilizers and accelerators.

The first hypophosphite based Pd plating bath had EDTA and EDA as the complexing agents to stabilize the solution (Sergienko, 1968). More stable baths were developed using NH_3 as the complexing agent and hypophosphite as the reducing agent (Pearlstein and Weightman, 1969). The plating bath stability was further improved by adding small amounts of thiosulfate ($Na_2S_2O_3 \cdot 5H_2O$) into Pearlstein and Weightman's bath (Zayats et al., 1973). Other hypophosphite based baths were used for corrosion protection in nuclear plants and chemical industries (Mizumoto et al., 1986; Vereshchinskii et al., 1973). The main drawback of hypophosphite based Pd baths is that phosphorous is included in Pd coating, thereby affecting the H_2 permeability of the membrane (Hough et al., 1981; Pearlstein and Weightman, 1969). Moreover, when removing substrates from plating bath, cracking appeared in the palladium layer due to H_2 gas production during plating (Cheng and Yeung, 2001; Pearlstein and Weightman, 1969). In fact, H_2 was produced

and adsorbed by the Pd layer when using hypophosphite. At the plating temperatures of 60-70°C, the β phase nucleated leading to distortions and cracking of the Pd layer.

The use of hydrazine as a reducing agent did not lead to the formation of H_2 but N_2, which avoided the cracking of the freshly deposited Pd film (Rhoda, 1959b; 1959a). Rhoda's plating bath stability was further improved by the addition of thiourea as the stabilizer (Kawagoshi, 1977). Formaldehyde was used to deposit Pd with strong acidic baths (Abys, 1964). Indeed, Pd is not a very good catalyst for formaldehyde oxidation at high pH (Ohno et al., 1985) yet it is at low pH. It was reported that $Pd(NH_3)(NO_3)_2$ led to a better Pd conversion than $Pd(NH_3)_4Cl_2$ and that pH should be between 9 and 11 for better solution stability (Keuler et al., 1977). Also, EDTA to Pd molar ratios between 20:1 and 40:1 and T> 65°C resulted in palladium salt conversion levels greater than 80 percent (Keuler et al., 1977).

Over the years electroless Pd plating baths and deposition conditions reached a common standard with small variations. Plating baths and deposition conditions are listed in Table 2.1.

Table 2.1 Pd plating bath and plating conditions commonly reported in the literature

Pd ion source	$Pd(NH_3)_4Cl_2 \cdot H_2O$, g/l	4–5
	or	
	$Pd(NH_3)(NO_3)_2$, g/l	0.35–15
Complexant, stabilizer	$Na_2EDTA \cdot 2H_2O$ g/l	40-80
Buffer, stabilizer	NH_4OH (28%), ml/l	200-650
Reducing agent	H_2NNH_2 (1 M), ml/l	4–10
pH		9–11.5
Temperature (°C)		50-70

In order to prepare a composite Pd membrane by the electroless deposition method the activated porous support is immersed in a Pd plating bath with the chemical composition

and at the conditions listed in Table 2.1. The reduction of Pd complexes, which depends on the composition of the bath, occurs at the surface of the activated support leading to a Pd deposit.

2.4 Composite Pd and Pd alloy membranes

This section describes the different types of supports onto which Pd is deposited by any of the techniques described in Section 2.2. In addition, a review on different composite Pd and Pd alloy membranes and their properties is given.

2.4.1 Supports and diffusion barriers used for metal composite membranes

The deposition of Pd, or any other H_2 permeable metal, onto a porous substrate forms a Pd or Pd alloy composite membrane. Vycor glass, porous metals (stainless steel, hastelloy, inconel) and ceramics (Al_2O_3, silica, TiO_2, zeolites) can all be used as porous substrates. Three important support properties have significant influences on the general performance of the Pd or Pd alloy membrane. These are: the nature (or chemical composition) of the support, porosity and pore size distribution at the surface.

The chemical composition of the support mainly affects the long term stability of the membrane. The use of metallic supports like Porous Stainless Steel (PSS) and Porous Hastelloy (PH) leads to intermetallic diffusion at high temperatures (usually above 300°C) unless a diffusion barrier is formed between the metallic support and the thin Pd film. Intermetallic diffusion is the migration of Fe, Cr, Ni and other elements from the support into the Pd layer, thereby affecting the H_2 permeation properties of the membrane. This problem is not encountered when using ceramics or Vycor glass.

Mostly oxides (including thin ceramic layers) have been used as intermetallic diffusion barriers. The passive film that naturally forms on Fe-Cr alloys is usually less than 50nm thick (Collins, 1998) yet does not protect against intermetallic diffusion at high temperatures and the treatment of the support is necessary before Pd deposition. Heat treatment of stainless steel at temperatures above 400°C led to an oxide layer that increases Pd membrane stability to over 6000 hr at 350°C (Ma et al., 1998). When the oxidation of 316L PSS supports was performed at temperatures lower than 400ºC H_2 permeance was found to decline (Guazzone et al., 2004). Oxides formed on 316L SS at temperatures equal or higher than 800ºC were found to be thick, 5-7μm, and consisting of a Cr rich oxide on top of a Fe rich oxide (Ma et al., 2004).

γ-Al_2O_3 was also widely used as intermetallic diffusion barrier (Nam and Lee, 2001; Yepes et al.). Nam and Lee (2001) covered a PSS disk first with nickel powder to obtain a smoother surface. After sintering under high vacuum at 800°C for 5 hr, they applied a thin γ-Al_2O_3 layer by the sol gel method. Two layers of Pd and two layers of Cu were sequentially deposited. The structure was then annealed to obtain an homogeneous Pd-Cu membrane. Long term H_2 flux stability was tested at 500°C for 960 hr and no H_2 flux decline was observed. Jun et al (2000) applied the same nickel powder on PSS disks but did not use γ-Al_2O_3. The Pd-Ni alloy membrane deposited on this Ni(powder)/PSS smooth support did exhibit more than 80% H_2 flux decline over a long period at 500°C (Jun and Lee, 2000). More recently, Yepes et al. (2005) obtained Pd-Ag membranes prepared by the coating and diffusion technique on PSS supports modified with γ-Al_2O_3. They proved with EDX techniques the absence of intermetallic diffusion although their H_2 permeance

was fairly low and equaled to 19 $m^3/(m^2\ h\ bar^{0.5})$ at 500ºC. The low H_2 permeability was in fact due to a relatively thick Pd-Ag layer of 16μm.

TiN layers with thicknesses ranging from 0.1 to 5μm, formed by sputter deposition inhibited the diffusion of Fe into the Pd-Ag dense film up to temperatures close to 700ºC (Shu et al., 1996). Recently, the TiN layer was also found to slightly improve the separation properties of Pd-Tin-PSS membranes (Nam and Lee, 2005). Nam and Lee (2005) prepared a Pd-Tin-PSS membranes with a submicron thickness having a H_2 permeance of around 52 $m^3/(m^2\ h\ bar^{0.5})$ and a selectivity of 4600 (H_2/N_2) at 450ºC. Both H_2 permeance and ideal selectivity were stable for over 40 days at 450ºC in H_2 atmosphere. The H_2 permeance was relatively high compared to other composite Pd membranes in the literature although very low for a composite Pd membrane having a submicron thickness. The low H_2 permeance was due to the large support resistance after deposition of the TiN layer. The rate at which intermetallic diffusion occurs in composite Pd membranes prepared on Porous Metallic (PM) supports was shown to be faster in H_2 atmosphere than in He atmosphere (Edlund and McCarthy, 1995).

The second important parameter, which is crucial for H_2 flux, is the support porosity or void fraction. Gas flow through porous media can be modeled using the Ergun equation, Equation (2-2)

$$\frac{\Delta P}{L} = \frac{150\mu(1-\varepsilon)u_0}{\varepsilon^3 d_p^2} + \frac{1.75(1-\varepsilon)\rho u_0^2}{\varepsilon^3 d_p} \qquad (2\text{-}2)$$

With ΔP the pressure drop, L the length of the porous media, μ the gas viscosity, ε the porosity or void fraction, u_0 the gas superficial velocity, d_p the particles diameter and ρ the gas density. For porous tubes, Equation (2-2) is valid if the thickness of the wall is

negligible when compared to the radius of the tube. For a given pressure drop, ΔP, the gas flow through the porous support can be increased if ε tends to 1 i.e. with high porosities. Therefore, high porosity supports are suitable for high H_2 flux. The limit for porosity is set by mechanical properties of the support. Porous supports with low porosity lead to composite Pd membranes with low H_2 permeance due to large mass transfer resistance within the supports. Vycor glass and ceramic supports have low inert gas permeances. The presence of mass transfer within the porous support has the effect of lowering the activation energy for H_2 permeation (Wang et al., 2004)

The maximum pore size on the surface of the support is the third crucial parameter (Ma et al., 2001). Ma et al. (2001) deposited a thin Pd layer on three PSS samples characterized by different grades: 0.1, 0.2 and 0.5 μm. Mercury intrusion analysis showed that: the lowest grade included the smallest maximum pore size on the surface and the highest grade included the largest maximum pore size on the surface. The Pd thickness needed to obtain a He tight membrane was shown to be approximately three times the diameter of the largest pore for the three membranes.

2.4.2 Asymmetric supports

In order to combine small pores on the surface and high porosity asymmetric supports can be used. An asymmetric support is a high porosity support covered by a second layer characterized by a small average pore size and a narrow pore size distribution. Thin Pd films of a few microns (Jayaraman and Lin, 1995; Li et al., 1996; Li et al., 1993; Uemiya et al., 1991b) were deposited on asymmetric γ-Al_2O_3/α-Al_2O_3 supports due to their small pore size on the surface (50-200 nm) and showed high H_2 flux due to low mass transfer resistance (support's pore size: 4–10 μm). Ni particles/PSS (Jun and Lee, 2000), γ-

Al_2O_3/Ni particles/PSS (Nam and Lee, 2001), ZrO_2/PSS (Wang et al., 2004) are also examples of asymmetric supports. Hence, it appears that the current trend is to modify by in-house techniques the bare porous support in such a way that a very smooth surface is achieved for the deposition of Pd.

Physical methods were also used to modify the surface of porous metal supports (Jemaa et al., 1996; She, 2000). Jemaa et al. (1996) obtained composite Pd membranes as thin as 6 μm on 0.5 μm grade PSS supports after shot peening the bare surface with 100μm in diameter Fe particles. However, they reported a H_2 permeance of 11.3 $m^3/(m^2\ h\ bar^{0.5})$ at 400ºC, which is low for a 6 μm thick membrane. No reason was given for such a low H_2 permeability. She (2000) obtained thin (20 μm) composite Pd membranes on 0.5 μm grade PSS supports by brushing the bare support with a metallic brush.

Wang et al. (2004) modified a 0.2 μm grade PSS support (Mott Corporation) with zirconium oxide. ZrO_2 was deposited from a colloidal solution by pulling a vacuum in the inside of the tube for 1 hr. After removing the excess ZrO_2 with water, the support was calcined at 300ºC for 2 hr. The ZrO_2 colloid-deposition and calcination procedure was repeated several times before activation and Pd deposition. A 10 μm thick Pd membrane was obtained after electroless deposition. The 10 μm composite Pd membrane on the ZrO_2/PSS modified support showed a H_2 permeance of 32.2 $m^3/(m^2\ h\ bar^{0.5})$ with a low selectivity (H_2/Ar) equal to 156. No reasons were reported for such a low selectivity.

PSS supports have recently been modified with SiO_2 colloid suspensions (Su et al., 2005), $Al(OH)_3$ and CeO_2 colloids (Tong et al., 2005a; Tong et al., 2005b; Tong et al., 2005c). Su et al. (2005) achieved H_2 permeabilities as high as 50 $m^3/(m^2\ h\ bar^{0.5})$ at 500ºC and ideal separation factors (H_2/N_2) of 300-450 on SiO_2 modified PSS supports.

The high fluxes were due to the thinness of the Pd layers, 2-6 μm, achieved on modified supports. Tong et al. (2005) achieved H_2 permeances ranging between 50-60 $m^3/(m^2\ h\ bar^{0.5})$ at 500ºC on modified PSS supports. Their composite Pd membrane was 6 μm thick. Unfortunately, none of the above-cited researchers carried out long-term H_2 permeance stability tests in order to elucidate the long-term H_2 permeance and ideal selectivity of their composite Pd membranes.

2.4.3 The use of an external driving force during deposition

Osmotic pressure carried the Pd complexes present in the plating solution deeper into the large pores of the substrate (Souleimanova et al., 2000; Souleimanova et al., 2002; Souleimanova et al., 2001; Yeung et al., 1995). Hence, the preferential deposition of Pd in deep "valleys" (large pores) resulted in the selective blocking of big defects. The small pores were then covered with a thin Pd layer producing a highly H_2 permeable membrane. Li et al. (1998) used electroless plating coupled with osmosis to prepare a 10 μm composite Pd membrane, with a low H_2 permeability of $18.7 \cdot 10^{-5}$ m^3 $m/(m^2\ h\ bar^{0.5})$ at 480ºC and a selectivity (H_2/N_2) in the range 1200-1600. Souleimanova et al. (2001) studied the effect of osmotic pressure on Pd particle size and showed that the particle size decreased when the osmotic pressure was increased and consequently, the Pd surface was smoother. The H_2 permeability of composite Pd membranes prepared with osmotic pressure was found to be higher (although by only 1.5 m^3 $m/(m^2\ h\ bar^{0.5})$) than the H_2 permeability of composite membranes prepared without osmotic pressure (Souleimanova et al., 2002), which was explained by the fact that finer Pd agglomerates were obtained at higher osmotic pressures. Souleimanova et al. (2002) also reported better mechanical stability under temperature cycling for membranes prepared by electroless plating and

osmosis on PSS. Furthermore, Pd went deeper in the PSS support increasing the adhesion of the membranes to the support.

It should be noted that membranes prepared with electroless plating coupled with osmosis had a lower permeability than membranes prepared with electroless plating. This was due to the fact that in membranes prepared using the electroless plating method coupled with osmosis, the thickness of the Pd layer was thicker than the determined value since Pd was forced into the pores.

2.5 The microstructure of Pd thin films from electroless deposition

The microstructure of composite Pd membranes was not extensively studied. It has been widely accepted that the fresh Pd layers deposited with electroless deposited method included very small Pd grains in the order of 10 nm (Li and Cheng, 1996; Souleimanova et al., 2002). Due to the presence of N_2 bubbles at the surface of the layer during plating, some microporosity was incorporated within the deposit (Yang et al., 2001). Also due to the low temperature (around 60ºC) at which electroless deposition method is carried out Pd columnar grains are expected (Müller, 1985). In fact, very little is known on the microstructure of Pd deposits besides grain size and microstrains. Pd films are suspected to have microporosity although no EXAFS studies were carried out to measure the size of microvoids in electroless Pd deposits (Babanov et al., 1997). Porosity and pore size can also be measured by Small Angle Neutrons Scattering (SANS) (Sanders et al., 1998).

Several researchers reported a possible effect of Pd grain size on H_2 permeance and their conclusions are varied. Some thought that small grains enhanced H_2 permeance (Bryden and Ying, 2002; Yan et al., 1994) while others believed that large crystallites led to high H_2 permeation (Li et al., 1998; McCool and Lin, 2001). The basis of the first

thought being "small crystallites lead to high H_2 fluxes" is the fact that for many metallurgical systems grain boundary diffusion is characterized by an activation energy lower than the activation energy of bulk diffusion by a factor of two. Using Quasielastic Neutron Scattering (QENS), H_2 diffusion was shown to be rapid within the grain boundaries in nanocrystalline palladium (Janßen et al., 1997). Also, at 20°C the H_2 diffusion coefficient of nano-Pd sample at low H_2 concentrations was lower than H_2 diffusion coefficient at low H_2 concentrations in Pd single crystal due to the trapping of H_2 atoms in high energy sites of the grain boundaries (Mütschele and Kirchheim, 1987). Once all these high energy sites in the grain boundaries have been filled (this occurred at higher concentrations) the diffusion coefficient of H_2 in nano-Pd became larger than the H_2 diffusion coefficient in single Pd crystals (Mütschele and Kirchheim, 1987). Finally at even higher H_2 concentrations the diffusion coefficient of H_2 in the nano-Pd starts to decrease due to H-H interactions inside the grain boundaries. Moreover, several researches found an increase in H_2 solubility in nanocrystalline Pd (Eastman et al.; Mütschele and Kirchheim, 1987; Wolf et al., 1994) that might contribute to an increase in H_2 permeability. The second thought being "large grains enhance H_2 permeation" is based on the fact that grain boundaries are seen as gaps where, to go from one grain to the other, H_2 needs to desorb and recombine on the surface of the first grain, travel as molecule through the boundary, readsorb and dissociate on the surface of the second grain and finally diffused in the lattice of the second grain. The effect of Pd grain size on H_2 permeability in composite Pd membranes is still unclear.

2.6 Leaks in composite Pd and Pd alloys membranes

At the present, a number of composite Pd membranes have been prepared by many researchers on Al_2O_3 supports, Vycor glass and PM supports. Many composite Pd membranes showed high H_2 permeance and good chemical stability. Indeed, even for composite Pd membranes on PM supports, new technologies decreased to a large extent the problems posed by intermetallic diffusion. However, leak stability over time is an issue that have not received too much attention but arises in all Pd composite membranes.

Leaks can form in composite Pd membranes due to "H_2 embrittlement". Originally, the term "H_2 embrittlement" was used to describe the shape, size and structure modifications (deformations) of freestanding Pd samples after several $\alpha-\beta-\alpha$ transformations (Lewis, 1967). β phase nucleation will not occur if care is taken to keep the conditions of the membrane in the stability region of the α phase, which is relatively easy to perform by adequately controlling the temperature and pressure. Therefore the α to β transformation poses little problem.

Reasons for leak formation and leak growth are in fact microstrains and stress release. Indeed, microstrains are present in fresh (or "green") membranes and are due to imperfections between Pd grain boundaries (Li and Cheng, 1996). Microstrains are released upon heating of the sample (Murakami, 1991). Stresses are denoted as intrinsic (Floro et al., 2001; Koch, 1994; Rajamani et al., 2002) when the causes of the formation of the stress are related to the material itself. Stresses caused by external factors are denoted as extrinsic. Extrinsic stresses are mostly due to thermal expansion coefficient mismatch between the film and the support (Murakami, 1991; Vook and Witt, 1965; Witt and Vook, 1968). Intrinsic and extrinsic stresses lead to either the expansion or contraction of

the Pd lattice parameter. The fundamental difference between microstrains and stresses is that microstrains are located at the Pd grain boundaries or at the external shell of Pd grains (Reimann and Wurschum, 1997), while stresses are due to contraction or expansion of the unit cell. When enough energy is given to the system, microstrains and stresses are relaxed and the structural changes that occur during stress relaxation (Floro et al., 2001) may play an important role in leak formation and leak growth.

The absorption of H_2 in a composite Pd membrane also leads to compressive extrinsic stresses denoted as H_2 stresses. The magnitude of compressive stresses after H_2 absorption depends on the H_2 loading n(H/Pd). Indeed, H_2 loading leads to the expansion of the Pd film (Baranowski et al., 1971). However, since the film is attached to the support, its expansion will be limited and compressive stresses will arise. Therefore, if the H_2 pressure is cycled at any temperature below 300ºC and, between a low pressure and a high pressure such that the miscibility gap boundary is closely approached, structural changes (dislocations, microcracks) may occur in the membrane after many cycles due to the repeated tensile/compressive stresses in the Pd layer.

Cycling H_2 pressure can have a degrading effect on composite Pd membranes (Checchetto et al., 2004). Checchetto et al. (2004) studied a 4 μm thick Pd/polycarbonate coated PSS at 100ºC and H_2 pressures ranging from 10 mbar to 195 mbar. They studied the mechanical stability of the composite membrane by switching 10 times H_2 and N_2 at 100ºC and a pressure difference of 100 mbar. They reported cracks on the Pd coating and attributed those cracks to $\alpha \rightarrow \beta \rightarrow \alpha$ phase transformations. However, at 100ºC, 200 mbar are needed to trigger the β phase nucleation. Therefore, switching gases at 100ºC and a pressure of 100 mbar was safe. However, what caused the membrane to fail were the re-

peated "extrinsic" tensile/compressive stresses. Also, the membrane may have failed during H_2 testing when the pressure was raised up to 195 mbar. Indeed, 195 mbar was very close to or even higher than the maximum pressure allowed at 100ºC. Nam and Lee (2001) studied the mechanical stability of a 2 μm PdCu/γ-Al_2O_3 coated PSS membrane by switching 18 times at 450ºC H_2 and N_2 atmospheres at a pressure difference of 0.7 bar. The total mechanical stability experiment lasted for 40 days. Nam and Lee (2001) reported no degradation of separation properties of the thin film. Tong et al. (2005) also cycled 40 times at 500ºC between H_2 (ΔP = 1 bar) and Ar atmosphere a 6 μm thick composite Pd $Al(OH)_3$-modified PSS membrane without seeing any deterioration in the separation properties of the membrane.

In many cases, pinholes were found on the surface of composite Pd membranes after characterization. These pinholes were attributed to the oxidation and reduction during membrane testing of some localized regions in the Pd layer and/or localized regions in the PSS support (Lee et al., 2003). Paglieri et al. (1999) suspected Sn impurities from the activation layer to be responsible for pinhole formation. Pinhole formation is far from being understood.

The lack of understanding in the leak formation and growth is partially due to the time it requires to follow a composite Pd membrane at different temperatures over a long period of time. Works in the literature only reported leak and selectivity data at one temperature from the measurement of a single leak rate. The difficulty in understanding the leak behavior of Pd composite membranes is also due to the complexity of different type of membranes studied where the dense layer could be Pd or Pd alloy, the intermediate layer could be an oxide formed in-situ or an oxide formed by the sol gel technique

and the support may be glass, Al_2O_3 or porous metals. A study on the role that stresses and stress release play on the leak formation is needed.

3 Experimental set-up and procedures

3.1 Composite Pd membranes synthesis

3.1.1 Porous metal supports

Two types of support geometries were used in this study: plates and cylindrical supports. The Porous Metal (PM) plates 1 cm ×1.5 cm were made out of 316L Stainless Steel, C22 Hastelloy or α-alumina (denoted as PSS plates, PH plates and α-Al_2O_3 plates). The Porous metal cylindrical supports were made out of 316L Stainless Steel or Hastelloy, with either 1.27 cm or 2.54 cm OD, variable length (2.54, 5.08 and 15.24 cm) and also denoted as PSS supports and PH supports. All porous metal supports were available in 0.1, 0.2 and 0.5 μm grade. The grade of a support is defined as follows: a support with a 0.5 μm grade rejects 95% of particles larger than 0.5μm in diameter.

PSS and PH plates were made by cutting a 100 cm^2 porous metal sheet into pieces of 1 to 1.5 cm^2. A small hole was drilled in a corner of the PSS and PH plates to hang them from hooks for activation and plating procedures. Cylindrical porous metal supports for composite Pd membranes were prepared by welding to one end of the PSS or PH tube a blind cap and welding a non-porous metal tube to the other end. A typical porous metal support for the fabrication of composite Pd membranes is shown in Figure 3.1.

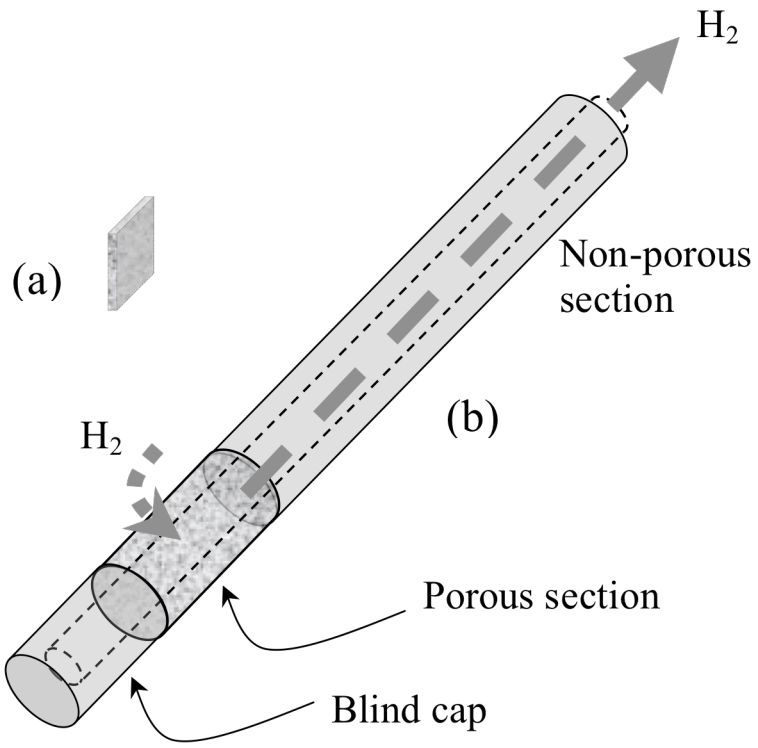

Figure 3-1 (a) PSS, PH or Al_2O_3 plate. (b) Assembly of a blind cap, porous metal tube and non-porous metal tube

The weld nugget between the blind cap and the porous metal tube was denoted as the "lower weld" and the weld nugget between the porous metal tube and the non-porous metal tube was denoted as the "upper weld". All porous metal plates and porous metal supports were purchased from Mott Corporation, Farmington, CT.

All PM supports were cleaned before oxidation, activation and Pd electroless deposition. The following cleaning procedure was used for every sample: 30 to 60 min. immersion in an alkaline solution (45 g/l NaOH, 65 g/l Na_2CO_3, 45g/l $Na_3PO_4 \cdot 12H_2O$), including 5ml/l of a saturated solution of industrial detergent, for dirt and grease removal. The samples were then thoroughly washed with De-Ionized Water (DI water) to remove the alkaline solution trapped in the pores of the supports. A strip of pH paper was stuck on the surface of the samples to check the acidity of the water remaining within the pores. The DI water cleaning step was repeated until the pH paper indicated 7. The last step involved a 10 min immersion in isopropanol (IPA) to hasten the drying of the supports. All the cleaning steps were carried out in an ultrasonic bath at 60°C. The supports were finally dried at 120°C overnight. After cleaning, the supports were oxidized in stagnant air at the desired temperature (10 to 12 hr at 400-600ºC for PSS supports and 12 hr at 700ºC for PH supports) to produce an oxide layer to prevent intermetallic diffusion. The mass of the bare support was measured before and after oxidation prior to any Pd plating. After oxidation, the He flux of the porous support was measured at different pressures in order to determine the initial He permeance.

3.1.2 Grading porous metal supports

After oxidation, the surface of most of the porous metal supports was smoothed by sequentially depositing coarse, fine and very fine pre-activated Al_2O_3 particles with

intermediate short Pd deposition to consolidate the powder. The process of making the surface of the porous metal support smoother was denoted as "grading" and is similar to the process yielding to asymmetric Al_2O_3 supports, where layers with different pore size are deposited by the sol gel process. The following grading procedure describes the steps followed for the grading of the support of membrane C01-F09. Any variation from this procedure was described when it occurred.

Three different mixtures of powders were prepared as described below.

Powder Mixture 1 included 65 wt% Al_2O_3 with an average particle size of 1 μm (Alfa Aesar); 30 wt% Al_2O_3 with an average particle size of 5 μm (Beuhler, Ltd.), and 5 wt% Al_2O_3 with an average particle size of 3 μm (Beuhler, Ltd.).

Powder Mixture 2 included 60 wt% Al_2O_3 with an average particle size of 0.3 μm (Alfa Aesar); 30 wt% Al_2O_3 with an average particle size of 3 μm (Beuhler, Ltd.), and 10 wt% Al_2O_3 with an average particle size of 1 μm (Alfa Aesar).

Powder Mixture 3 included 60 wt% Al_2O_3 with an average particle size of 0.01-0.02 μm (Alfa Aesar); 30 wt% Al_2O_3 with an average particle size of 1 μm (Alfa Aesar), and 10 wt% Al_2O_3 with an average particle size of 0.3 μm (Alfa Aesar).

Each powder was placed in a separate 500 ml cylinder containing 250 ml of aqueous $SnCl_2$ solution (1 g/l, pH=2). This step of sensitizing the powder was performed in an ultrasonic bath at 60ºC for 10 minutes. After 10 minutes, 250 ml of aqueous $PdCl_2$ solution (0.1 g/l, pH=2) were added into the cylinder already containing the aqueous $SnCl_2$ solution and Al_2O_3 powder. The resulting slurry, with a total volume of about 500 ml, became brown instantly. The slurry was placed in an ultrasonic bath at 60ºC for 10 minutes. The resulting surface activated powder was then filtered from the slurry by using one filter

paper (WHATMAN® GF/F type) for every 50 ml of slurry. The filter cakes were dried at 120ºC for 2 hr.

The fine and very fine mixtures of Al_2O_3 powders (*i.e.*, Powder Mixtures 2 and 3) were activated separately following the procedure described above. The coarse powder (*i.e.*, Powder Mixture 1) was not activated to avoid subsequent deposition of Pd too deep into the pore system of the PSS support.

The oxidized PSS support was placed for 1 minute in a 200 ml water slurry at pH 2 that contained 0.5 g of Powder Mixture 1. A vacuum was applied to the tube side of the support and an Al_2O_3 cake easily formed on the support.

Pd adhesion to the support is increased by the presence of anchoring sites. Anchoring sites, such as the tips of the substrate particles (*e.g.*, the tips of 316L SS particles[1] forming the PSS support), should not be covered by the Al_2O_3 powder for good adhesion between the Pd membrane and the support. To expose the anchoring sites, the extra Al_2O_3 cake was removed by gloved hand while gently rinsing with distilled water. The vacuum in the tube side was maintained during the removal of the extra Al_2O_3. Al_2O_3 remained inside the pores mouth of the porous support.

Following the deposition of Powder Mixture 1, the support was immersed for 1 minute in a 200 ml water slurry that contained 0.5 g of pre-activated Powder Mixture 2 while a vacuum was applied to the tube side of the support. Again, extra Al_2O_3 cake was removed carefully by gloved hand as described above. After deposition of the pre-activated Powder Mixture 2, the support was placed in 140 ml of Pd plating solution for 5 minutes of Pd plating (with no vacuum applied to the tube side) to glue the Al_2O_3 particles. Fol-

[1] The anchoring sites or tips of 316L SS (or PH) particles are shown in Figure 6-3, page 144

lowing the deposition of Powder Mixture 2, the support was immersed in a 200 ml water slurry that contained 0.5 g of pre-activated Powder Mixture 3 for 1 minute while a vacuum was applied to the tube side of the support. Again, extra Al_2O_3 cake was removed carefully by gloved hand. After the deposition of the pre-activated Powder Mixture 3, the support was immersed in 140 ml of Pd plating solution for 5 minutes of Pd plating (with no vacuum applied to the tube side). This process produced a graded support. The graded support was dried overnight at 120ºC and weighed. Also, the He leak at different pressures was measured in order to determine the He permeance after the grading step.

3.1.3 Support activation

Through out this study, the activation process was performed using sequential dipping in $SnCl_2$-HCl (1 g/l, pH 2) and $PdCl_2$-HCl (0.1 g/l, pH 2) solutions. Tin chloride dihydrate ($SnCl_2 \cdot 2H_2O$, 98% ACS) and Pd chloride ($PdCl_2$, 99.9%, metal basis, Assay) used for the preparation of the activation solutions, were purchased from Aldrich and Alfa Aesar respectively. The preparation of $SnCl_2$ solution consisted of putting 1 ml of HCl 10 mol/l (30%) into 10 - 20 ml of Di water, adding 1 g of $SnCl_2 \cdot 2H_2O$, shaking and finally adding Di water up to 1 l. The preparation of $PdCl_2$ solution consisted of putting 1 ml of HCl 10 mol/l (30wt%) into 100 ml of Di water, adding 0.1 g of $PdCl_2$, heating the solution to 60-80ºC until complete dissolution of the $PdCl_2$ salt and finally adding Di water up to 1 l. The $PdCl_2$ solution could be stored for long periods of time (months), on the other hand, $SnCl_2$ solution had always to be prepared just before the activation since aging of the $SnCl_2$ solution led to polymeric substances within the solution (Reva and Vorob'eva, 2002).

3.1.4 Pd plating solution

The Pd plating solution included $Pd(NH_3)_4Cl_2 \cdot H_2O$ as the Pd source, Na_2EDTA as the complexing agent, NH_3OH as the buffer and NH_2-NH_2 (hydrazine) as the reducing agent. The Pd plating bath did not include any accelerator or stabilizer to keep the chemistry simple. The bath composition used for Pd deposition is listed in Table 3-1.

Table 3-1 Pd plating bath and deposition conditions for membrane preparation

$Pd(NH_3)_4Cl_2 \cdot H_2O$	4 g/l	99.9% (metal basis), Alfa Aesar
$Na_2EDTA\ 2H_2O$	40.1 g/l	99+%, Aldrich
NH_4OH	198 (ml/l)	28wt%, Merck
H_2NNH_2 (1 M)	5.7 ml/l	99 wt%, Aldrich
pH	10-11	
Temperature	60°C	

One liter of the Pd plating solution was prepared by first, adding 198 ml of ammonium hydroxide to 200 ml of Di water. Secondly, 4 g of $Pd(NH_3)_4Cl_2\ H_2O$ were added and the solution was shaken until complete dissolution of the Pd salt. 40.1 g of Na_2EDTA were added in a third step and the solution was stirred for 20-30 min until complete dissolution of the Na_2EDTA. Finally, Di water was added to the total volume of one liter. Pd plating solutions were prepared 24 hr before use to let the system reach an equilibrium state. Hydrazine was added into the plating solution right before the activated support was immersed in the plating bath. Even though Pd plating solutions could be stored for long periods of time, Pd plating solutions not older than 1-2 weeks were used for the preparation of composite Pd membranes.

3.1.5 Pd deposition on activated substrates

Pd deposition was carried out by immersing the activated support into the Pd plating bath for 90 minutes at 60ºC. After 90 minutes of Pd plating, the support was placed in Di water at the same temperature (60ºC) and let cool to room temperature. The plating solution was changed in the plating cell, hydrazine was added to the new plating solution and the support was reintroduced in the plating bath after a short rinsing of the plated surface with Di water. Sessions of 90 minutes Pd plating were carried out 2 to 4 times after activation. After Pd deposition, the support was thoroughly rinsed with Di water and let dry overnight at 120ºC. The Pd plating rate ranged from 0.5 μm/h to 3 μm/h and was mainly dependent on the ratio of the volume of Pd plating solution over the activated surface. For example, the simultaneous deposition of Pd onto four small plates (3 cm^2 per plate) was performed in a 100 ml beaker with 70 ml of plating solution ($R_{vol/surf}$ = 5.8 ml/cm^2) at a plating rate of around 2 μm/hr. Composite Pd membranes with a porous surface of 120 cm^2 were plated in a 500ml graduate cylinder with 400 ml of Pd plating solution ($R_{vol/surf}$ = 3.3 ml/cm^2) at a plating rate of around 1 μm/h. The activation-plating procedure was repeated until the composite Pd membrane became dense. The composite Pd membrane was assumed dense when the He permeance was lower than 10^{-4} $m^3/(m^2\ h\ bar)$ at room temperature and at a pressure difference of 1 bar. During the plating procedure, vacuum was created in the tube side of the membrane using an aspirator when the He permeance of the membrane reached 1 $m^3/(m^2\ h\ bar)$ in order to easily block the last remaining large pores.

The thickness of the Pd thin film was determined by the gravimetric method i.e. weight gain of the sample divided by the product of the plated surface area and the metal

density. Gravimetric methods gave an average thickness value for the membrane generally in good agreement with the thicknesses determined by SEM pictures. Table 3-2 summarizes all the membranes prepared for this study.

Table 3-2 List of all membranes studied in this work

Membrane	Support type (μm-alloy)	Area (cm^2)	Ox.Temp (ºC)	Support grade layer	Pd thickness Gravimetric (μm)	Pd thickness SEM (μm)
C01-F03	0.1-PSS	8.4	400	No	32	37
C01-F04	0.1-PSS	8.4	none	No	28	28
C01-F05	0.1-PSS	8.4	500	No	33	Not determined
C01-F06	0.1-PSS	23	600	No	19	21
C01-F07	0.1-PSS	23	500	No	23	24
C01-F08	0.1-PSS	23	500	Yes	15	19-24
C01-F09	0.1-PSS	23	500	Yes	14	14-15
C01-F11a	0.1-PSS	23	500	Yes	10	Not determined
C01-F11b	C01-F11	23	500	Yes	13	17
C02-F01	0.2-PSS	23	500	No	37	Not determined
C02-F03	0.2-PSS	23	500	No	37	Not determined
Ma-32	0.1 medium-PH	120	700	Yes	7.7	Not determined
Ma-32b	Ma-32	120	-	Yes	10	Not determined
Ma-32c	Ma-32b	120	-	Yes	12	12-14
Ma-34	0.1 coarse-PH	120	700	Yes	4	Not determined
Ma-34b	Ma-34	120	-	Yes	8	9.4
Ma-41	0.1 coarse-PH	120	700	Yes	10	Not determined
Ma-42	0.1 medium-PH	120	700	Yes	5.6	Not determined

3.2 The determination of H_2 permeance in composite Pd membranes

3.2.1 H_2 permeation set-up

The H_2 permeation characterization of the composite Pd membranes with small H_2 permeable surface (8.4 and 23 cm^2) was performed in a "small" unit. The H_2 permeation characterization of composite Pd membranes with large H_2 permeable surface (120 cm^2) was performed in a "large" unit. The only differences between the "small" and the "large" units were the size of the furnaces, the size of the ballast volumes and the range of H_2 and He digital mass flow meters. However, the functionality and layout of both units was the same and is shown schematically in Figure 3-2.

The permeation set-ups consisted of a tube furnace and a stainless steel reactor where the membrane was housed in a shell-and-tube arrangement and sealed with stainless steel and graphite ferrules. The temperature was monitored in the tube side of the membrane and controlled by a separate J type thermocouple located on the outside wall of the stainless steel reactor for safety purposes. A temperature controller (Eurotherm type 2116) was used to control the temperature at the reactor wall and adjusted to have the desired temperature at the tube side. A Type 600A MKS pressure transducer was used to measure the pressure in the tube side and a second transducer, type 727A MKS, was placed at the shell side to monitor the H_2 inlet pressure. Inert gas flow rates (leaks) through the membrane were measured with a digital mass flow meters with 10 ("small" unit) or 50 ("large" unit) sccm[1] range (MKS M10MB model), specially calibrated for He.

[1] sccm= standard cm^3 per minute

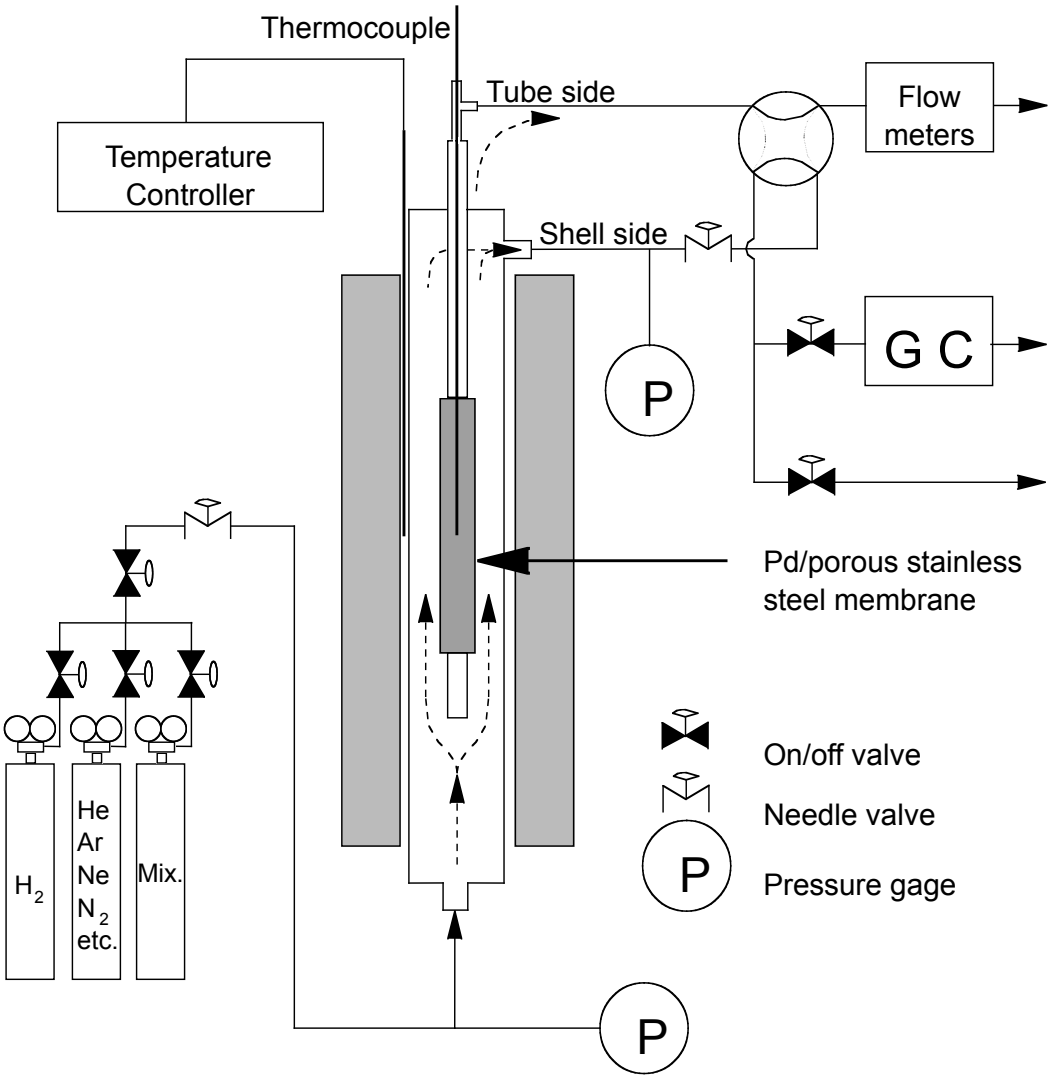

Figure 3-2 H_2 permeation set-up

When the leaks were measured with other gases such as Ar or N_2 bubble flow meters with different ranges were used. The H_2 flux was measured using a second digital mass flow meter with 200, 500 and 1000 sccm range in the "small" unit and 5000 or 20000 sccm range (MKS M10MB model) in the "large" unit. All H_2 digital mass flow meters were specially calibrated for H_2 gas. All parameters, tube temperature, pressures and flows were logged continuously into a computer using a TBX-68T Terminal block (National Instruments) data acquisition box and NI 4351 high precision voltage meter (National Instruments). Ballast volumes (500 ml to 6000 ml depending on the permeation unit) in the inlet side permitted a gradual change of the composition of the gas to be purged (He to H_2 or H_2 to He). A He sweep line was also used at the tube side of the membrane to keep at all times the H_2 partial pressure at the tube side lower than the H_2 partial pressure at the shell side while changing from H_2 to He. Therefore, the tube-side purge avoided any back flow of H_2 from the tube side to the shell side while changing from H_2 to He. Any small amount of H_2 back flow might cause the membrane to fail. All membranes were tested using Ultra High Purity (UHP) H_2 gas purchased from Aimtek Inc., Auburn, MA.

3.2.2 Typical characterization procedure for a composite Pd membrane

The general characterization procedure of a composite Pd membrane involved:

(1) The heating of the membrane in He atmosphere (P_{shell}=2 bar) from room temperature to 250ºC at a rate of 1ºC/min. A small tube purge (10-40 sccm) was also established to remove water vapor from the tube side. At 250ºC the tube purge was stopped.

(2) The measurement of the leak (He, Ar and N_2) at 250ºC at several different pressures.

(3) The introduction of H_2 at 250ºC and a pressure of 2 bar.

(4) A dwell time in H_2 atmosphere ranging from 1 to 4-5 days during which the H_2 pressure difference was kept equal to 1 bar (2:1). During the dwell time, the H_2 permeance was determined 1 to 3 times. For each time the H_2 permeance was determined, the H_2 flux was measured at 10-15 different pressures within the 1-4.4 bar pressure interval at the shell. The permeate pressure was always kept equal to atmosphere.

(5) The switching from H_2 to He at 250ºC to measure the leak (He) at 250ºC. Typically, the He leak after the H_2 test at 250ºC was different from the He leak before the H_2 test. The He leak was measured at 5-10 different pressures.

(6) The switching in atmosphere from He to H_2 at 250ºC.

(7) A dwell time of 5 hr[1] to reach the previous H_2 permeance at 250ºC.

(8) The change in temperature from 250 to 300ºC at a rate of 1ºC/min or slower in H_2 atmosphere.

(9) Steps (3), (4), (5), (6), (7) and (8) were repeated at 300, 350, 400, 450 and 500ºC.

(10) The membrane was cooled from 500ºC to 250ºC in H_2 atmosphere.

(10) The atmosphere change at 250ºC from H_2 to He and the cool down from 250ºC to room temperature at a rate of 1ºC/min.

All membranes studied in this work were characterized according to the above-described procedure. However, some steps, such as measuring the He leak or the H_2 per-

[1] hr = hours

meance at a given temperature, were omitted for some membranes. For instance, some membranes were tested at temperatures higher than 500ºC. For some membranes, the He leak at a given temperature was measured 4 to 5 times in order to measure the rate at which the He leak increased as a function of time at a given temperature. Also, for some membranes (Ma-32b/41) H_2 permeance was monitored for times longer than 4-5 days to study the long-term stability of the composite Pd membranes prepared in this study.

3.2.3 The determination of H_2 permeance

The H_2 permeance was determined by three different methods. The first method was based on the measurement of a single H_2 flux at a given pressure difference. H_2 permeance, F_{H2}, was estimated by dividing the single H_2 flux, J_{H2}, by the difference of the square root of the high pressure, $P^{0.5}{}_{shell}$, and the low pressure side, $P^{0.5}{}_{tube}$, as shown in Equation (3-1).

$$J_{H_2} = F_{H2} \cdot (P_{shell}^{0.5} - P_{tube}^{0.5}) \qquad (3\text{-}1)$$

F_{H2} was only used to follow the permeance as a function of time, which in fact corresponded to follow H_2 flux as a function of time during dwell times. F_{H2} was particularly used to determine the activation energy for H_2 permeation by monitoring H_2 flux as the temperature was changed, which is explained in Section 3.2.4.

The second method to determine the H_2 permeance was based on the measurement of H_2 flux at 10-15 different pressure differences (ΔP=0.2-3.5 bar). The 10-15 J_{H2} values were plotted as a function of $\Delta(P^{0.5})$ and the data (J_{H2}, $\Delta(P^{0.5})$) were then fitted with a linear regression assuming the n-exponent equal to 0.5 using Equation (3-2).

$$J_{H_2} = F_{0.5} \cdot (P_{shell}^{0.5} - P_{tube}^{0.5}) \qquad (3\text{-}2)$$

The H_2 permeance determined assuming Sieverts' law was denoted as $F_{0.5}$.

Finally, the third method was based on the measurement of H_2 flux at 10-15 different pressure differences (ΔP=0.2-3.5 bar). The 10-15 (J_{H2}, P_{shell}, P_{tube}) data points were then fitted with a non-linear regression given by Equation (3-3). Hence, the experimental data were fitted with the F_n and the n-exponent parameters.

$$J_{H_2} = F_n \cdot (P_{shell}^{n-\exp onent} - P_{tube}^{n-\exp onent}) \quad (3\text{-}3)$$

The H_2 permeance determined assuming P^n dependence of the H_2 flux was denoted as F_n. The regression of the experimental data (linear and non-linear) was performed by the least squares method, i.e. minimizing the Sum of the Squares of the Residuals (SSR) shown in Equation (3-4).

$$SSR = \sum_{i=1}^{N} (J_{H2,\exp}^{i} - F_{0.5,n} \cdot ((P_{shell,\exp}^{i})^n - (P_{tube,\exp}^{i})^n)^2 \quad (3\text{-}4)$$

The subscript "*exp"* in Equation (3-4) stands for experimental.

3.2.4 Determination of the activation energy for H_2 permeance

Two different methods were used to determine the activation energy for H_2 permeation through composite Pd-PM membranes:

(1) Determining the steady state values of H_2 permeance, $F_{0.5}$, at all temperatures (250, 300, 350, 400, 450 and 500ºC) after allowing the membrane to dwell in H_2 atmosphere for long times, 20 to 100 hr. Experimental values were then plotted in an Arrhenius plot ($Ln(F_{0.5})$, 1/T) and fitted with a straight line.

(2) Measuring the H_2 flux, J_{H2}, as a function of temperature while changing temperature at a very slow rate of 1°C/min. During the temperature change the pressure difference was kept constant and equal to 1 bar (2:1). Temperature changes were

performed by increments of 50ºC. Since the logging data terminal box was set to log all system parameters every 3 minutes, a total of 16 experimental (J_{H2}, Temp.) points were collected for every temperature change. Experimental values were then plotted in an Arrhenius plot ($Ln(J_{H2})$, 1/T) or ($Ln(F_{H2}=J_{H2}/(\sqrt{2}-1))$, 1/T) and fitted with a straight line.

3.3 Leaks in composite Pd membranes

3.3.1 Leak measurements and ideal separation factor

Leaks in composite Pd membranes were most of the times measured with He. N_2 and Ar were used for only specific experiments, which are detailed in their respective sections. The measurement of the He leak consisted of determining the He permeance. Hence, at any given temperature, the He flow was measured at the following pressure differences: 1, 1.5, 2, 2.5, 3 and 3.5 bar. The permeate side pressure was always kept at the atmospheric conditions. The He permeance was then determined by fitting the (He flux, ΔP) experimental points with Equation (3-5)

$$J_{He} = He_{permeance} \cdot \Delta P \qquad (3\text{-}5)$$

where J_{He} is the He flux in $m^3/(m^2\ h)$, $He_{permeance}$ is the permeance of the He leak in $m^3/(m^2\ h\ bar)$ and ΔP the pressure difference in bar. The ideal separation factor, denoted as selectivity, was defined by the ratio of the H_2 flux and the He flux at the same pressure difference. Since, the H_2 flux was proportional to $\Delta(P^{0.5})$ and the He flux was proportional to ΔP, the selectivity value depended on the pressure considered. In this work, all reported selectivities were determined at a pressure difference of one bar according to Equation (3-6).

$$Selectivity = \left(\frac{J_{H_2}}{J_{He}}\right)_{\Delta P=1} = \frac{F_{0.5}\cdot(\sqrt{2}-\sqrt{1})}{He_{permeance}} \quad (3\text{-}6)$$

In addition, the experimental data (J_{He}, ΔP) was plotted in the form (J_{He}, P_{ave}), where P_{ave} was the average transmembrane pressure equal to (P_{shell}+P_{tube})/2. Plotting (J_{He}, P_{ave}) allowed for the determination of the average pinhole[1] diameter, the total pinhole surface and the total number of pinholes. The calculations leading to pinhole diameter, total pinhole surface and number of pinholes are described in Chapter 10, Section 10.3.1.

[1] Pinholes: defects with the shape of a little hole that form in the dense Pd layer of a composite Pd membrane at high temperatures. The size and formation of these features are discussed in Chapter 10

3.3.2 Leak distribution along the membrane length

The distribution of leaks in large membranes (15 cm long, 2.54 cm OD, area=120cm^2) was studied by means of a "rising water test". The set-up, shown in Figure 3-3, and concepts used for this experiment were kindly transmitted from the research team at Shell International Exploration and Production, Inc., Huston, TX. The composite Pd membrane was housed in a Plexiglas shell and sealed with rubber O rings. A scale, divided in cm, was printed on the wall of the Plexiglas tube. The membrane was placed in such a position that the lower weld matched with the "zero" mark of the printed scale. A water reservoir was placed at a higher level than the plastic cell and connected via Tygon® tubing to the plastic cell. A on/off valve (valve A) allowed the admission of water to the plastic cell.

A pressurized He tank was connected to the plastic cell via stainless steel tubing and a 3-way valve (valve B) such that the inlet of the 3-way valve was connected to the plastic cell, the first outlet of the valve B was connect to the He tank and the second outlet of valve B was open to the atmosphere.

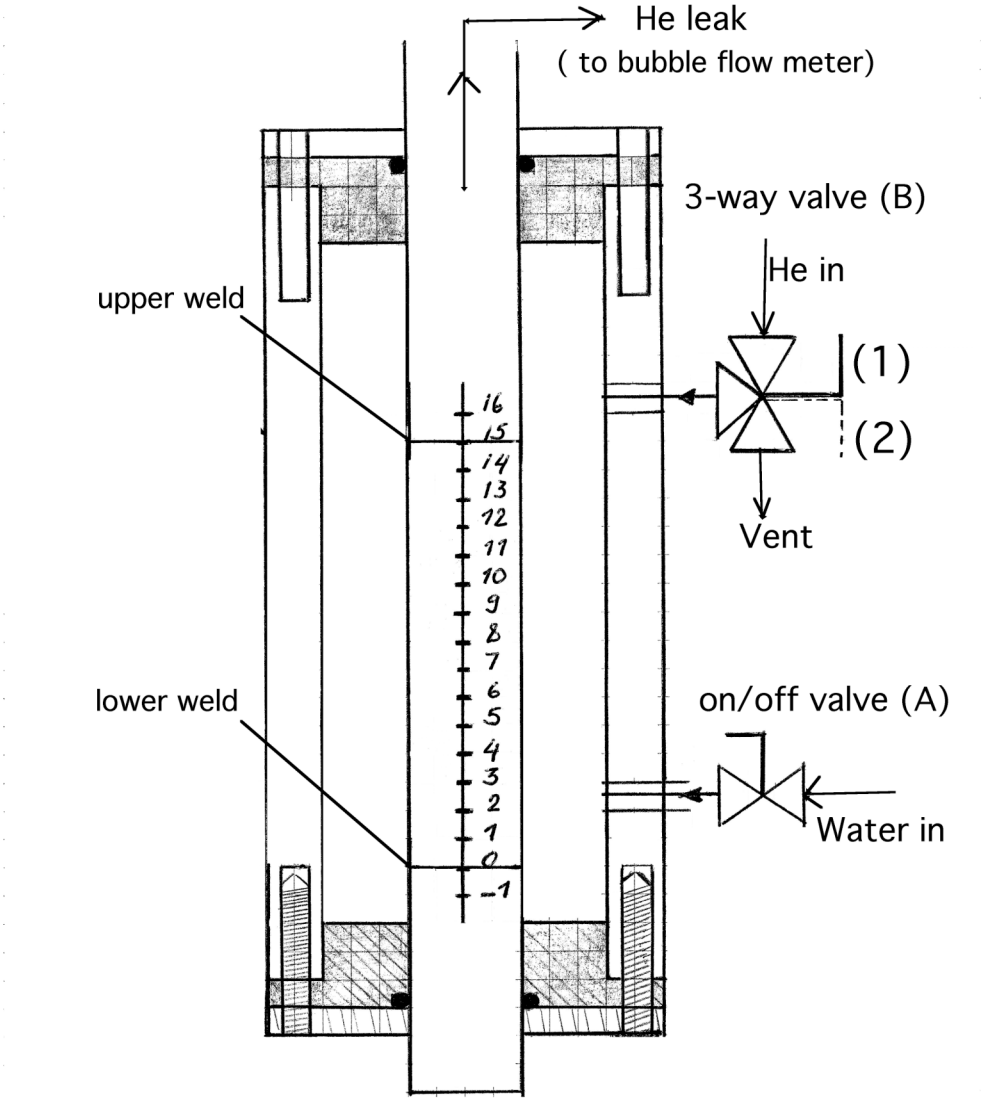

Figure 3-3 "Rising water test" apparatus (Shell International Exploration and Production, Inc.)

The leak distribution along the composite Pd membrane was determined as follows:

(1) At atmospheric pressure (3-way valve B in position 2), the on/off water valve (valve A) was opened to let water flow into the Plexiglas shell until the water meniscus reached the "-1" mark. At the "-1" mark the on/off valve A was closed.

(2) He was then introduced into the shell by switching the 3-way valve (valve B) to position 1. The He leak was measured with a bubble flow meter at a given pressure difference. Since the water was at the "-1" mark, the first leak measurement corresponded to the total leak of the membrane.

(3) The pressure in the shell was then released by switching the 3-way valve to position 2 and the water level was increased up to the "0" cm mark by opening the on/off water valve A. At the "0" mark the leak equaled the leak at the "-1" mark, however, sometimes, due to capillary forces water flowed above the lower weld and clogged some cracks and defects in the welding area resulting in a lower He leak. The leak at "-1" ensured the true total leak of the membrane.

(5) He was reintroduced into the shell and the He leak of the membrane was measured.

The procedure was repeated until the water level reached the last mark where the He leak was zero.

3.4 Microstructure characterization methods

3.4.1 Scanning Electron Microscope (SEM)

Surface characterization was performed using an Amray 1610 Turbo Scanning Electron Microscope (SEM) coupled with Energy Dispersion X-Ray (EDX) capabilities (Princeton Gamma-Tech Instruments Inc., Rocky Hill, NJ). The EDX detector was

equipped with a beryllium window allowing the detection of light elements. Atom and weight concentration profiles were determined with the Spirit software (Princeton Gamma-Tech Instruments Inc., Rocky Hill, NJ).

Elemental composition (line-scans) was performed at an acceleration potential of 10, 15 or 20 kV, 39 mm working distance, 33º tilt and a 5-10 minutes dwell time. The spatial resolution increased as the accelerating voltage was decreased and equaled 0.3 μm at 15 kV. Most of the elemental composition analysis were performed at 15 kV.

3.4.2 X-ray diffraction (XRD) techniques

XRD was used to investigate the microstructure (grain size and strains), "intrinsic" and "extrinsic" stresses in electrolessly deposited Pd coatings. Also, time dependent processes such as nucleation, phase growth and alloying in Pd-Cu alloys were studied using a time resolved X-ray diffractometer. Hence, three X-ray diffractometers were used for the analysis of thin Pd deposits. A Rigaku Geigerflex located at Worcester Polytechnic Institute (WPI), a PANalytical X'Pert Pro MPD located at Oak Ridge National Laboratories (ORNL) and a time resolved High Temperature XRD also located at ORNL. The PANalytical X'Pert Pro MPD and the High Temperature X-ray diffractometers located at ORNL site were used for macro-stresses measurements and strain release in Pd films and monitoring of phase transformations in Pd-Cu alloys respectively. The Rigaku diffractometer located at WPI was mainly used for grain size-strain measurements and general phase characterization.

XRD techniques and theory, grain size, strain and stress calculations were covered in detail by several researchers (Cullity and Stock, 2001; Klug et al., 1954). A brief theory

on strain-size and stress determination is given in Chapter 9, although, the reader is encouraged to consider Cullity and Klug manuals for a complete understanding.

3.4.2.1 Time resolved phase transformations, High Temperature X-Ray Diffraction

High-Temperature X-Ray Diffraction (HTXRD) was used as a major technique allowing the real-time monitoring of microstructure and phase transformations with respect to temperature and time. The time resolved HTXRD, with copper radiation ($\lambda CuK\alpha$=1.540598Å), was composed of a Scintag PAD X vertical θ/θ goniometer, a Buehler HDK 2.3 furnace and a mBraun linear position sensitive detector (LPSD). The data were collected in a multichannel analyzer (MCA) with the active area of the detector defined by about 500 channels at a resolution of 0.02º/channel corresponding to an angular range of 10º 2θ window. The data from the MCA were downloaded to the computer in 2 sec allowing fast data collection. For instance, a perfect well defined Pd XRD pattern could be taken in just 2 minutes while an hr would have been needed to collect the same Pd XRD pattern on the Rigaku Gegerflex diffractometer. The programmed heating/cooling procedure was controlled precisely and flexibly (heating and cooling rates up to 300ºC/min) through a computer using a thin Pt/10%Rh heater strip[1] and a Pt/Pt-13%Rh thermocouple welded to the Pt/10%Rh heater strip. When thin films on top of the thick substrates were studied, for instance, Pd thin films on 2 mm thick α Al_2O_3 substrates, a second Pt/10%Rh heating strip bent around the sample was used to better control the temperature and overcome the temperature gradient within the substrate.

[1] The heater strip was also the sample holder.

However, the presence of such heater did not permit a pyrometric temperature measurement of the thin film on the substrate. Therefore, temperature calibration of the furnace was performed by correlating the temperature given by the thermocouple and the real temperature deduced from the lattice parameter of silver powder placed on an uncoated $\alpha-Al_2O_3$ substrate. The Ag lattice parameter was measured at four different temperatures in the 200-800ºC temperature range (Touloukian et al., 1977). The calibrating line, thermocouple temperature vs. real temperature shown in Figure 3-4, was then obtained in He atmosphere. A difference in temperature, not larger than 50ºC, was observed between the Pd thin film and the Pt-Rh heater strip due to the low thermal diffusion coefficient of α-Al_2O_3 substrate. To avoid Pd or Cu oxidation He was flowed through a high temperature Ta strips purifier to avoid oxygen contamination.

The atmosphere in the stainless-steel sample chamber could be tailored with various gases (inert, oxidative, or reductive) for specific experimental needs. Data acquisition and analysis were performed using DMS-NT software (Scintag, Inc., Cupertino, California) and Jade 6 software (Materials Data, Inc., Livermore, California).

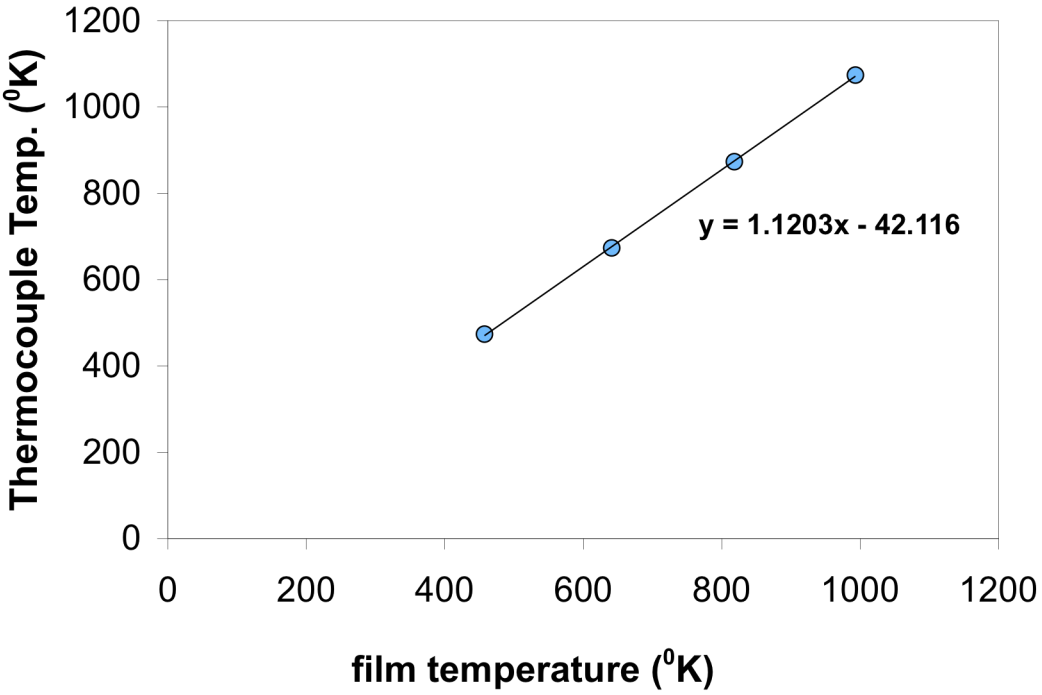

Figure 3-4 Temperature calibration curve when using a surround heater.